

# The Carotid Body Detects Circulating Tumor Necrosis Factor-Alpha to Activate a Sympathetic Anti-Inflammatory Reflex

Pedro L. Katayama<sup>1</sup>, Isabela P. Leirão<sup>1</sup>, Alexandre Kanashiro<sup>2</sup>, João Paulo M. Luiz<sup>3</sup>, Fernando Q. Cunha<sup>3</sup>, Luiz C. C. Navegantes<sup>4</sup>, Jose V. Menani<sup>1</sup>, Daniel B. Zoccal<sup>1</sup>, Débora S. A. Colombari<sup>1</sup> & Eduardo Colombari<sup>1</sup>

## Affiliations

<sup>1</sup>Department of Physiology and Pathology, School of Dentistry, São Paulo State University, Araraquara, São Paulo, Brazil.

<sup>2</sup>Department of Neurosciences and Behavior, Ribeirão Preto Medical School, University of São Paulo, Ribeirão Preto, São Paulo, Brazil

<sup>3</sup>Department of Pharmacology, Ribeirão Preto Medical School, University of São Paulo, Ribeirão Preto, São Paulo, Brazil.

<sup>4</sup>Department of Physiology, Ribeirão Preto Medical School, University of São Paulo, Ribeirão Preto, São Paulo, Brazil.

## Corresponding authors

Pedro L. Katayama & Eduardo Colombari  
Department of Physiology and Pathology, School of Dentistry, São Paulo State University, Rua Humaita, 1680, Centro, Araraquara/SP, Brazil – Postal code: 14801-903. emails: katayamapl@gmail.com; eduardo.colombari@unesp.br

39 **Abstract**

40 Recent evidence has suggested that the carotid bodies might act as immunological  
41 sensors, detecting pro-inflammatory mediators and signalling to the central nervous  
42 system, which, in turn, orchestrates autonomic responses. Here, we demonstrated  
43 that the TNF- $\alpha$  receptor type I is expressed in the carotid bodies of rats. The systemic  
44 administration of TNF- $\alpha$  increased carotid body afferent discharge and activated  
45 glutamatergic neurons in the nucleus tractus solitarius (NTS) that project to the rostral  
46 ventrolateral medulla (RVLM), where the majority of pre-sympathetic neurons reside.  
47 The activation of these neurons was accompanied by generalized activation of the  
48 sympathetic nervous system. Carotid body ablation blunted the TNF- $\alpha$ -induced  
49 activation of RVLM-projecting NTS neurons and the increase in splanchnic  
50 sympathetic nerve activity. Finally, plasma and spleen levels of cytokines after TNF- $\alpha$   
51 administration were higher in rats subjected to either carotid body ablation or  
52 splanchnic sympathetic denervation. Collectively, our findings indicate that the carotid  
53 body detects circulating TNF- $\alpha$  to activate a counteracting sympathetic anti-  
54 inflammatory mechanism.

55

56 **Keywords:** Carotid Body; Sympathetic Nervous System; Inflammation; Neuroimmune  
57 Interactions; Neuroimmunomodulation; Neural Circuits

58

59

60

61

62

63

64

65

66

67

68

69

70

71

## 72 **Introduction**

73 The existence of neuroimmune interactions and their relevance to the control of  
74 inflammation are well-established and have been extensively explored in the last 20  
75 years (Abe et al., 2017; Araujo et al., 2019; Bassi et al., 2020; Chavan et al., 2017;  
76 Chu et al., 2020; Gabanyi et al., 2016; Kressel et al., 2020; Lankadeva et al., 2020;  
77 Martelli et al., 2014; Murray et al., 2021; Steinman, 2004; Tanaka et al., 2021) since  
78 the discovery of the “inflammatory reflex” (Borovikova et al., 2000). In general, there  
79 is a consensus that this reflex works as a negative-feedback mechanism that  
80 comprises: 1) a detection component, which identifies pathogen- or danger-associated  
81 molecular patterns, generating an inflammatory response; 2) an afferent arm, which  
82 conveys information about the systemic inflammatory status to the central nervous  
83 system; 3) integrative centers in the brain, that receive and process signals regarding  
84 the systemic inflammatory condition, orchestrating an appropriate counteracting  
85 response and; 4) an efferent arm, which are the effectors that exert immunomodulatory  
86 functions to promote resolution of infection and inflammation.

87 The vagus nerve is considered an important element in neuroimmune  
88 interactions (Borovikova et al., 2000; Kressel et al., 2020). Its afferent (sensory) and  
89 efferent (motor) fibers are involved in the bidirectional communication between the  
90 nervous and the immune systems, providing a reflex mechanism known as the  
91 “cholinergic anti-inflammatory pathway” (Borovikova et al., 2000). According this  
92 mechanism, vagal sensory neurons detect inflammatory mediators produced in  
93 conditions of systemic inflammation and send this information to the central nervous  
94 system (Watkins et al., 1995), which, in turn, generates a vagal efferent output that  
95 counteracts inflammation mainly through acetylcholine-induced inhibition of cytokine  
96 production (Borovikova et al., 2000). The importance of this cholinergic anti-  
97 inflammatory mechanism is beyond doubt since its dysfunction is involved in the  
98 pathophysiology of several conditions (Bassi et al., 2017; Chang et al., 2019;  
99 Kanashiro et al., 2017; Li et al., 2011; van Maanen et al., 2009). However, several  
100 studies have shown convincing evidence for the existence of other neural mechanisms  
101 that regulate inflammation. For instance, animal and human studies have  
102 demonstrated that the efferent sympathetic nervous system can modulate  
103 inflammatory conditions through catecholamine-mediated suppression of innate  
104 immune responses (Abe et al., 2017; Kox et al., 2014; Lankadeva et al., 2020; Martelli

105 et al., 2014; Tanaka et al., 2021; van Westerloo et al., 2011). Moreover, some studies  
106 demonstrated that the sympathetic-mediated anti-inflammatory reflexes do not  
107 depend on vagal afferent signalling, suggesting the existence of other peripheral  
108 mechanisms able to detect inflammation and communicate with the central nervous  
109 system to activate downstream sympathetic anti-inflammatory pathways (Abe et al.,  
110 2017; Martelli et al., 2014).

111 In this regard, the carotid body, classically known as the main peripheral  
112 monitor of the O<sub>2</sub> levels in the blood, has been considered a polymodal sensor due to  
113 its particular ability to detect diverse molecules present in the circulation, such as  
114 glucose, sodium chloride, hormones, and also, inflammatory mediators (Allen, 1998;  
115 da Silva et al., 2019; Jendzjowsky et al., 2018; Katayama, 2016; Kumar and  
116 Prabhakar, 2012; Thompson et al., 2016). In the context of inflammation, several  
117 pieces of evidence indicate that the carotid bodies might be involved in the intricate  
118 interplay between the immune system and the sympathetic nervous system. First, the  
119 carotid body expresses receptors for inflammatory mediators such as  
120 lysophosphatidic acid (LPA) and pro-inflammatory cytokines such as IL-1 $\beta$ , IL-6, and  
121 tumor necrosis factor-alpha (TNF- $\alpha$ ) (Fernández et al., 2008; Jendzjowsky et al., 2018;  
122 Kumar and Prabhakar, 2012; Mkrtchian et al., 2012; Wang et al., 2002). Second, LPA  
123 and pro-inflammatory cytokines stimulate the carotid body and increase the carotid  
124 sinus nerve (CSN) afferent activity in isolated *in vitro* preparations (Jendzjowsky et al.,  
125 2021, 2018). Third, carotid body stimulation by its typical stimulus (hypoxia) activates  
126 central autonomic areas that control parasympathetic (Erickson and Millhorn, 1994;  
127 Zera et al., 2019) and, also, the sympathetic nervous system (Kline et al., 2010;  
128 Koshiya and Guyenet, 1996; Luise King et al., 2012) which, besides vagally-mediated  
129 mechanisms, represents an important component in the neural regulation of immunity  
130 (Abe et al., 2017; Lankadeva et al., 2020; Martelli et al., 2014). Last, carotid body  
131 denervation worsens systemic inflammation and accelerates multiple organ  
132 dysfunction and death in rats with lipopolysaccharide (LPS)-induced sepsis (Nardocci  
133 et al., 2015), suggesting that the carotid body is a protective factor during acute  
134 inflammatory conditions. Altogether, these observations led to the hypothesis that the  
135 carotid body plays a role in neuroimmune interactions, but the exact mechanisms  
136 underlying this cross-talk are largely unknown.

137 In this study, we focused on investigating the impact of TNF- $\alpha$  (a ubiquitous  
138 cytokine that triggers inflammation)(Grieve et al., 2017) on the carotid body-mediated

139 activation of the sympathetic nervous system, as well as the relevance of this  
140 interaction in the modulation of TNF- $\alpha$ -induced systemic inflammation. We revealed  
141 that the carotid body expresses the TNF- $\alpha$  receptor type I (TNFR1) and detects  
142 increased levels of TNF- $\alpha$  in peripheral circulation, transmitting this information to the  
143 brain via CSN afferent inputs to commissural nucleus tractus solitarius (cNTS)  
144 glutamatergic neurons that project to rostral ventrolateral medulla (RVLM) pre-  
145 sympathetic neurons, resulting in activation of the sympathetic nervous system to  
146 counteract the TNF- $\alpha$ -induced inflammation. We, therefore, propose the existence of  
147 a physiological carotid body-mediated neuroimmune reflex that acutely controls  
148 inflammation. The identification of this neuroimmune reflex provides potential  
149 mechanistic insights into the pathophysiology of inflammation-mediated diseases as  
150 well as into the development of novel therapeutic strategies to treat these conditions.

151

152

153

154

155

156

157

158

159

160

161

162

163

164

165

166

167

168

169

170

171

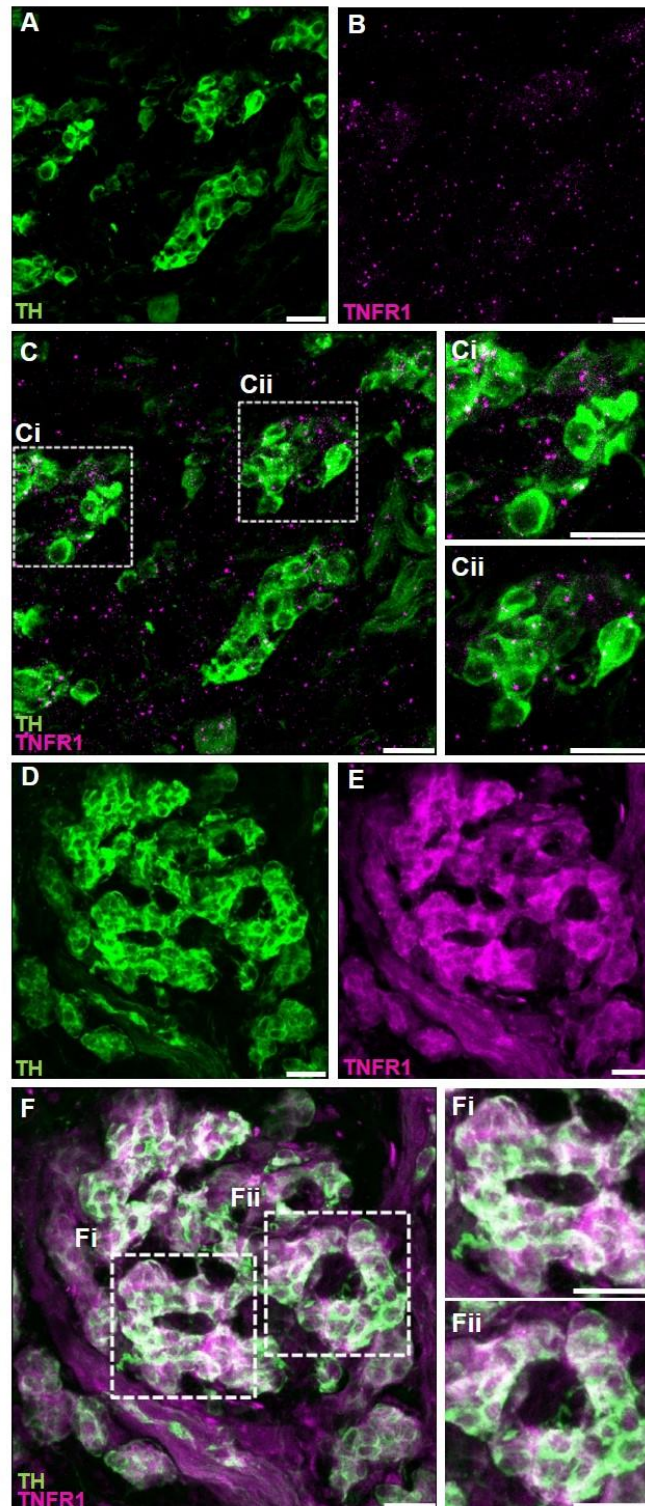
172 **Results**

173

174 **TNFR1 is expressed in the carotid body**

175 The expression of TNF- $\alpha$  receptors type I (TNFR1) in the carotid body was verified  
176 using two different methods: 1) RNAscope *in situ* hybridization for labelling TNFR1  
177 mRNA molecules combined with immunofluorescence staining for tyrosine  
178 hydroxylase (TH) to identify carotid body glomus cells (Fig. 1A – C) and; 2) double  
179 immunofluorescence staining for TNFR1 and TH (Fig. 1D – F). We found that the  
180 TNFR1 is expressed in the carotid body of rats at both mRNA and protein levels (Fig.  
181 1).





182

183 **Figure 1.** TNF- $\alpha$  receptors type I (TNFR1) are expressed in the carotid body of rats. **A – C.** Combined  
184 fluorescent *in situ* hybridization (TNFR1, magenta puncta) and immunofluorescence (Tyrosine  
185 hydroxylase, TH, green staining). **A.** TH positive cells (glomus cells) in the carotid body. **B.** RNAscope  
186 *in situ* hybridization showing TNFR1 mRNA expression in the carotid body. **C.** Overlay of images A and  
187 B showing the colocalization of TH and TNFR1. **Ci** and **Cii.** Zoom into selected regions of image C. **D**  
188 **– F.** Double immunofluorescence staining (TNFR1, magenta staining; and TH, green staining). **D.** TH  
189 positive cells (glomus cells) in the carotid body. **E.** TNFR1 expression in the carotid body. **F.** Overlay of  
190 images D and E showing the colocalization of TH and TNFR1. **Fi** and **Fii.** Zoom into selected regions  
191 of image F. Scale bars: 20  $\mu$ m.  
192

193 **Circulating TNF- $\alpha$  increases carotid sinus nerve afferent activity**

194 Next, we investigated if elevated TNF- $\alpha$  levels in the blood could activate its receptors  
195 in the carotid body and increase CSN activity in vivo. We found that exogenous TNF-  
196  $\alpha$  administration increased CSN activity by  $34 \pm 5\%$  at 30 minutes after administration  
197 compared to baseline (Figure 2B). This TNF- $\alpha$ -induced excitation of CSN was  
198 sustained and lasted the whole experiment ( $46 \pm 7\%$ ,  $55 \pm 8\%$ ,  $60 \pm 10\%$  at 60, 90,  
199 and 120 minutes after TNF- $\alpha$  administration, respectively; Figure 2B). It is important  
200 to highlight that throughout the experimental protocol, the animals were artificially  
201 ventilated with a slight hyperoxia (50% O<sub>2</sub>, balance N<sub>2</sub>) avoiding any potential hypoxia  
202 episode. We also performed additional experiments which demonstrated that the  
203 intravenous TNF- $\alpha$  did not affect the partial pressure of oxygen (PaO<sub>2</sub>), the partial  
204 pressure of carbon dioxide (PaCO<sub>2</sub>), the pH, and the bicarbonate (HCO<sub>3</sub><sup>-</sup>)  
205 concentration in the arterial blood of unanesthetized, spontaneously breathing rats,  
206 confirming that the treatment does not produce hypoxia, hypercapnia or acidosis.  
207 (figure supplement 1). Thus, our data indicate that TNF- $\alpha$  can stimulate the carotid  
208 body and increase CSN activity independently of changes in blood gases and pH  
209 alterations. We, therefore, hypothesized that this TNF- $\alpha$ -induced increase in CSN  
210 afferent activity could activate central pathways similar to those activated by hypoxic  
211 stimuli, generating autonomic responses such as the activation of the sympathetic  
212 nervous system.

213

214

215

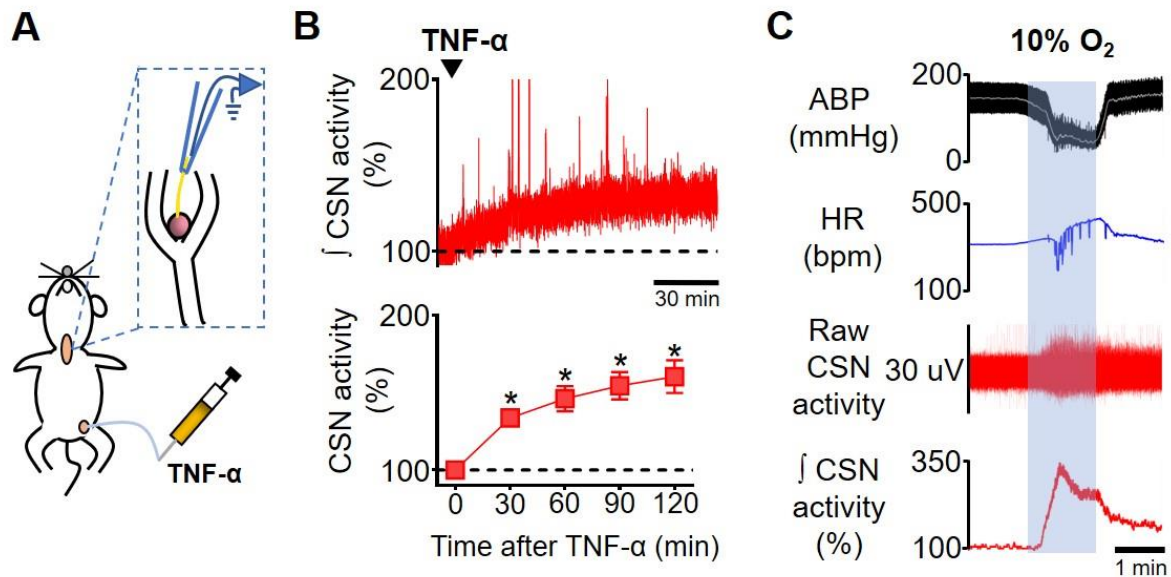
216

217

218

219





220

221 **Figure 2.** Carotid sinus nerve afferent activity (CSN activity) in response to intravenous TNF- $\alpha$ . **A.**  
222 Schematic illustration of the experimental protocol. **B.** Representative trace of the integrated CSN  
223 activity ( $\int$  CSN activity; time constant = 1 s) from one rat during baseline and after TNF- $\alpha$  (500 ng, IV,  
224 black arrowhead) administration (top; scale bar = 30 minutes) and summary data showing CSN activity  
225 at baseline and 30, 60, 90 and 120 minutes after TNF- $\alpha$  administration (bottom; n = 6). Baseline CSN  
226 activity was normalized to 100% after noise subtraction. A one-way repeated measures ANOVA  
227 detected statistically significant differences in CSN activity over time,  $F_{(4, 20)} = 21,282$ ,  $p < 0.001$ .  
228 Subsequent post hoc analysis with a Bonferroni adjustment revealed that, as compared to time 0  
229 (baseline), CSN activity was statistically significantly higher at 30 minutes (34%, 95% CI [9, 59],  $p =$   
230 0.014); at 60 minutes (46%, 95% CI [8, 85],  $p = 0.023$ ); at 90 minutes (55%, 95% CI [13, 96],  $p = 0.016$ );  
231 and at 120 minutes (60%, 95% CI [10, 111],  $p = 0.023$ ) after TNF- $\alpha$  administration. \* $p < 0.05$ . Data are  
232 means  $\pm$  SEM. **C.** Representative traces showing the viability of CSN activity recordings assessed by  
233 a brief exposure to hypoxia (10% O<sub>2</sub>, balance N<sub>2</sub>; grey shaded area). The typical acute response of  
234 urethane-anesthetized rats to hypoxia includes hypotension, bradycardia, and a robust increase in CSN  
235 activity. ABP, arterial blood pressure; HR, heart rate.

236

237

238

239

240

241

242

243

244

245

246

247

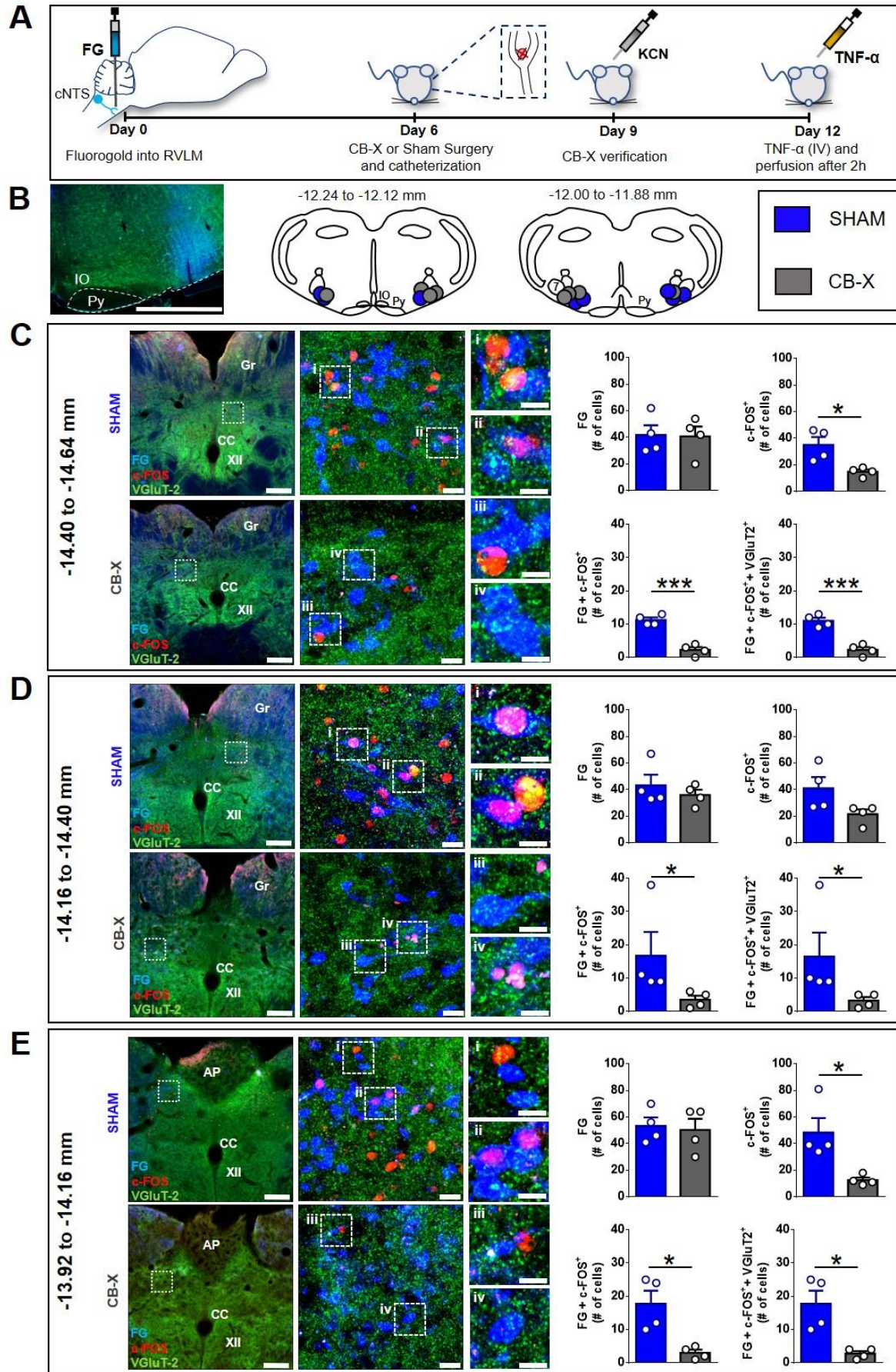
248

249

## 250 **RVLM-projecting cNTS glutamatergic neurons are activated by TNF- $\alpha$**

251 The first synapse of carotid body afferents within the central nervous system occurs in  
252 the cNTS, as extensively described in the literature (Colombari et al., 1996; Cruz et  
253 al., 2010; Kline et al., 2010; Malheiros-Lima et al., 2020). The cNTS sends excitatory  
254 glutamatergic projections to several areas, being implicated in diverse physiological  
255 functions. In the context of the carotid body-related functions, the cNTS neurons  
256 project to important autonomic areas involved in the neural control of cardiovascular  
257 and respiratory functions (Kline et al., 2010; Zera et al., 2019). For example, a previous  
258 report demonstrated direct monosynaptic projections from cNTS to RVLM, where the  
259 majority of pre-sympathetic neurons are located (Kline et al., 2010). It was also shown  
260 that most of these RVLM-projecting cNTS neurons are activated by hypoxia and  
261 constitute the major neural pathway of hypoxia-induced sympathetic activation (Kline  
262 et al., 2010; Koshiya and Guyenet, 1996). Thus, we sought to investigate if this  
263 sympathoexcitatory pathway is activated by circulating TNF- $\alpha$  since this cytokine  
264 increased the discharge of carotid body afferents, as shown in Figure 2B. Our results  
265 demonstrated massive monosynaptic projections from cNTS to RVLM (FG-labeled  
266 cells, blue staining, Figure 3C – E) in both SHAM and CB-X rats at all evaluated rostro-  
267 caudal levels: -14.40 mm to -14.64 mm (SHAM,  $42 \pm 7$  cells; CB-X,  $41 \pm 7$  cells), -  
268 14.16 mm to -14.40 mm (SHAM,  $43 \pm 8$  cells; CB-X,  $36 \pm 4$  cells), and -13.92 mm to -  
269 14.16 mm. (SHAM,  $53 \pm 6$  cells; CB-X,  $50 \pm 8$  cells). Most of these projections are  
270 excitatory (VGLUT2<sup>+</sup> cells, green staining, Figure 3C – E). Circulating TNF- $\alpha$  activated  
271 a considerable proportion of these RVLM-projecting glutamatergic cNTS neurons in  
272 SHAM rats, as indicated by c-FOS expression (red staining) in FG<sup>+</sup>/VGLUT2<sup>+</sup> cells  
273 (Figure 3C – E); Importantly, the number of activated RVLM-projecting glutamatergic  
274 cNTS neurons was dramatically reduced by carotid body ablation: -14.40 mm to -14.64  
275 mm (SHAM,  $11 \pm 1$  cells; CB-X,  $2 \pm 1$  cells), -14.16 mm to -14.40 mm (SHAM,  $17 \pm 7$   
276 cells; CB-X,  $3 \pm 1$  cells), and -13.92 mm to -14.16 mm. (SHAM,  $18 \pm 4$  cells; CB-X,  $3$   
277  $\pm 1$  cells). The efficacy of the bilateral carotid body ablation procedure was confirmed  
278 by the lack of cardiovascular responses to KCN (figure supplement 2A – B). Together  
279 with our previous findings (Figures 1 and 2), these results suggest that the carotid  
280 body detects the circulating TNF- $\alpha$  through TNFR1 and transmits this information to  
281 the central nervous system via carotid sinus nerve afferents, resulting in the activation  
282 of a sympathoexcitatory pathway.

283





286 **Figure 3.** Activation of RVLM-projecting cNTS glutamatergic neurons by circulating TNF- $\alpha$  in SHAM  
287 and CB-X rats. **A.** Schematic illustration of the experimental protocol. **B.** Representative image from a  
288 typical retrograde tracer (Fluorogold; FG) injection-site into RVLM and schematic pictures of RVLM  
289 injections-sites of all bilaterally FG-injected animals (n=4 per group). IO, inferior olive; Py, pyramidal  
290 tract; 7, facial motor nucleus. Scale bar is 1000  $\mu$ m. **C, D** and **E.** Images are representative pictures of  
291 cNTS sections at three different rostro-caudal levels, processed for c-FOS (red) and VGluT2 (green)  
292 immunofluorescence, and containing FG-positive cells retrogradely labeled from the RVLM (blue). Gr,  
293 gracile nucleus; CC, central canal; XII, hypoglossal nucleus; AP, area postrema. Scale bars are 200  
294  $\mu$ m for 5x magnification pictures (left), 20  $\mu$ m for 40x magnification pictures (middle) and 10  $\mu$ m for  
295 zoom pictures (right). **i, ii, iii,** and **iv.** Digital zoom into selected regions. Bar graphs show the  
296 quantification of retrogradely labeled FG neurons, c-FOS<sup>+</sup> neurons, double stained (FG/c-FOS<sup>+</sup>)  
297 neurons and triple stained (FG/c-FOS<sup>+</sup>/VGluT2<sup>+</sup>) neurons in the cNTS 2 hours after TNF- $\alpha$   
298 administration (500 ng, IV) in SHAM (n=4) and CB-X (n=4) rats. The number of RVLM-projecting  
299 neurons (FG-labeled cells) was not different between SHAM and CB-X rats in all evaluated cNTS levels:  
300 -14.40 to -14.64 mm (C),  $t(6) = 0.096$ ,  $p = 0.926$  (Student's  $t$ -test); -14.16 to -14.40 mm (D),  $U = 7.5$ ,  $z$   
301  $= -0.145$ ,  $p = 0.886$  (Mann-Whitney  $U$ -test); and -13.92 to -14.16 mm (E),  $t(6) = 0.285$ ,  $p = 0.785$   
302 (Student's  $t$ -test). General neuronal activation (i.e., both RVLM-projecting and RVLM- non-projecting;  
303 c-FOS<sup>+</sup> cells) was higher in SHAM as compared to CB-X rats at -14.40 to -14.64 mm (C),  $t(3.505) =$   
304  $3.326$ ,  $p = 0.036$  (Welch's  $t$ -test) and at -13.92 to -14.16 mm (E),  $U = 0$ ,  $z = -2.323$ ,  $p = 0.029$  (Mann-  
305 Whitney  $U$ -test); but not at -14.16 to -14.40 mm (D),  $t(6) = 2.141$ ,  $p = 0.076$  (Student's  $t$ -test). The  
306 specific activation of RVLM-projecting neurons (c-FOS<sup>+</sup>/FG<sup>+</sup> cells) was higher in SHAM as compared to  
307 CB-X rats in all 3 cNTS levels: -14.40 to -14.64 mm (C),  $t(6) = 7.919$ ,  $p < 0.001$  (Student's  $t$ -test); -14.16  
308 to -14.40 mm (D),  $U = 0$ ,  $z = -2.323$ ,  $p = 0.029$  (Mann-Whitney  $U$ -test); and -13.92 to -14.16 mm (E),  
309  $t(3.324) = 3.661$ ,  $p = 0.030$  (Welch's  $t$ -test). Virtually all activated RVLM-projecting cNTS neurons are  
310 glutamatergic (FOS<sup>+</sup>/FG/VGluT2<sup>+</sup> cells). The number of activated RVLM-projecting cNTS glutamatergic  
311 neurons was higher in SHAM as compared to CB-X rats in all 3 cNTS levels: -14.40 to -14.64 mm (C),  
312  $t(6) = 7.000$ ,  $p < 0.001$  (Student's  $t$ -test); -14.16 to -14.40 mm (D),  $U = 0$ ,  $z = -2.337$ ,  $p = 0.029$  (Mann-  
313 Whitney  $U$ -test); and -13.92 to -14.16 mm (E),  $t(3.219) = 3.755$ ,  $p = 0.029$  (Welch's  $t$ -test). \* $p < 0.05$   
314 and \*\*\* $p < 0.001$ . Data are means  $\pm$  SEM.

315

316

317

318

319

320

321

322

323

324

325

326

327

328

329

330

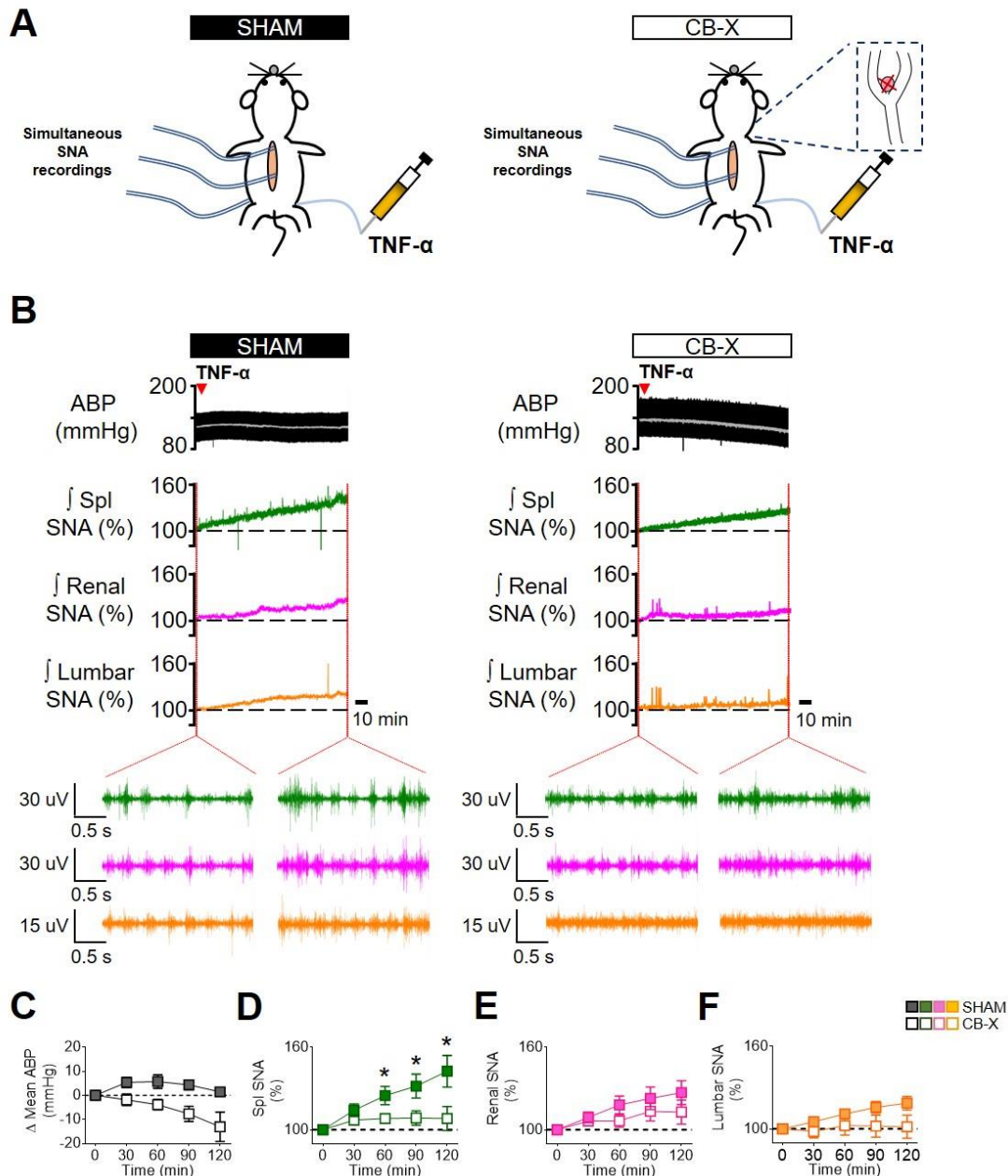
331

### 332 **TNF- $\alpha$ promotes a carotid-body mediated increase in splanchnic SNA**

333 Because circulating TNF- $\alpha$  activated a well-known sympathoexcitatory central  
334 pathway, we next performed experiments to investigate the effect of this cytokine on  
335 sympathetic activity directly recorded from multiple sympathetic nerves in vivo. Our  
336 results showed that intravenously administered TNF- $\alpha$  promotes a generalized  
337 sympathoexcitation in SHAM rats (Figure 4B – F), consistent with the activation of the  
338 RVLN-projecting cNTS glutamatergic neurons demonstrated in Figure 3:  $\Delta$  Splanchnic  
339 SNA ( $14 \pm 4\%$ ,  $25 \pm 7\%$ ,  $32 \pm 9\%$  and  $42 \pm 11\%$  respectively at 30, 60, 90, and 120  
340 minutes after TNF-  $\alpha$  administration);  $\Delta$  Renal SNA ( $9 \pm 4\%$ ,  $18 \pm 6\%$ ,  $22 \pm 8\%$ ,  $27 \pm$   
341  $9\%$  respectively at 30, 60, 90, and 120 minutes after TNF-  $\alpha$  administration) and  $\Delta$   
342 lumbar SNA ( $5 \pm 1\%$ ,  $11 \pm 3\%$ ,  $16 \pm 4\%$ ,  $19 \pm 5\%$  respectively at 30, 60, 90, and 120  
343 minutes after TNF-  $\alpha$  administration). Interestingly, despite the generalized  
344 sympathetic activation, mean arterial blood pressure (ABP) only slightly increased  
345 (Figure 4B – C).

346 Since carotid body ablation almost abolished the TNF- $\alpha$ -induced activation of  
347 RLVM-projecting cNTS glutamatergic neurons (Figure 3), we tested whether the  
348 carotid bodies would be necessary to the observed sympathoexcitation in response to  
349 TNF- $\alpha$  administration. To accomplish that, we administered TNF- $\alpha$  to rats subjected to  
350 bilateral carotid body ablation (Figure 4B – F). CB-X rats displayed an attenuated  
351 increase in SNA in response to TNF- $\alpha$ :  $\Delta$  Splanchnic SNA ( $7 \pm 1\%$ ,  $8 \pm 2\%$ ,  $8 \pm 5\%$   
352 and  $8 \pm 9\%$  respectively at 30, 60, 90, and 120 minutes after TNF- $\alpha$  administration),  $\Delta$   
353 renal SNA ( $6 \pm 3\%$ ,  $6 \pm 5\%$ ,  $13 \pm 7\%$  and  $13 \pm 9\%$  respectively at 30, 60, 90, and 120  
354 minutes after TNF-  $\alpha$  administration), and  $\Delta$  lumbar SNA ( $-2 \pm 5\%$ ,  $2 \pm 7\%$ ,  $2 \pm 8\%$  and  
355  $1 \pm 8\%$  respectively at 30, 60, 90, and 120 minutes after TNF-  $\alpha$  administration). These  
356 SNA responses were diminished compared to those displayed by SHAM rats,  
357 especially on splanchnic SNA at 60, 90, and 120 minutes after TNF-  $\alpha$  administration,  
358 suggesting that the carotid bodies contribute to this specific response (Figure 4D).  
359 Unlike SHAM rats, mean ABP in CB-X rats tended to decrease even without  
360 reductions in the activity of any of the recorded sympathetic nerves (Figure 4B – C).  
361 At the end of the experiments, bilateral carotid body ablation was confirmed by the  
362 lack of sympathetic and blood pressure responses to KCN (figure supplement 3A –  
363 B).

364



365

366 **Figure 4.** Carotid body ablation attenuates the TNF- $\alpha$ -induced splanchnic sympathetic activation. **A.**  
 367 Schematic illustration of the experimental protocol. **B.** Representative traces of arterial blood pressure  
 368 (pulsatile ABP, black; mean ABP, white), splanchnic (Spl; green), renal (magenta) and lumbar (orange)  
 369 integrated ( $\int$ ; time constant = 1s) sympathetic nerve activity (SNA) in sham-operated rats (SHAM) and  
 370 carotid body-ablated rats (CB-X) during baseline conditions and in the next 2 hours after TNF- $\alpha$   
 371 administration (500 ng, IV, red arrowhead). For each sympathetic nerve, raw SNA signals at baseline  
 372 and 2 hours after TNF- $\alpha$  administration are also presented (as indicated by the red dotted lines). **C, D,**  
 373 **E and F.** Summary data showing the changes in mean ABP (**C**), Spl SNA (**D**), Renal SNA (**E**)  
 374 and Lumbar SNA (**F**) in response to TNF- $\alpha$  in SHAM (filled symbols, n = 6) and CB-X (open symbols, n = 6)  
 375 rats. For each rat, baseline integrated SNA was normalized to 100%, and the relative changes were  
 376 calculated at four different time points (30, 60, 90 and 120 minutes after TNF- $\alpha$  administration). A  
 377 statistically significant group x time interaction on spl SNA was detected by two-way repeated-measures  
 378 ANOVA,  $F_{(3,15)} = 11.119$ ,  $p < 0.001$ . Subsequent simple main effects analyses revealed that spl SNA  
 379 changes were significantly greater in SHAM as compared to CB-X rats at 60 minutes,  $F_{(1,5)} = 7.042$ ,  $p$   
 380  $= 0.045$ ; at 90 minutes,  $F_{(1,5)} = 10.224$ ,  $p = 0.024$ ; and at 120 minutes,  $F_{(1,5)} = 16.515$ ,  $p = 0.010$  after  
 381 TNF- $\alpha$  administration. \* $p < 0.05$ . There were no statistically significant group x time interactions on  
 382 Mean ABP,  $F_{(1,113, 5,567)} = 0.807$ ,  $p = 0.420$ ,  $\epsilon = 0.371$ ; Renal SNA,  $F_{(3,15)} = 0.805$ ,  $p = 0.510$ ; and Lumbar  
 383 SNA,  $F_{(3,15)} = 1.685$ ,  $p = 0.213$  (two-way repeated measures ANOVA). Data are means  $\pm$  SEM.

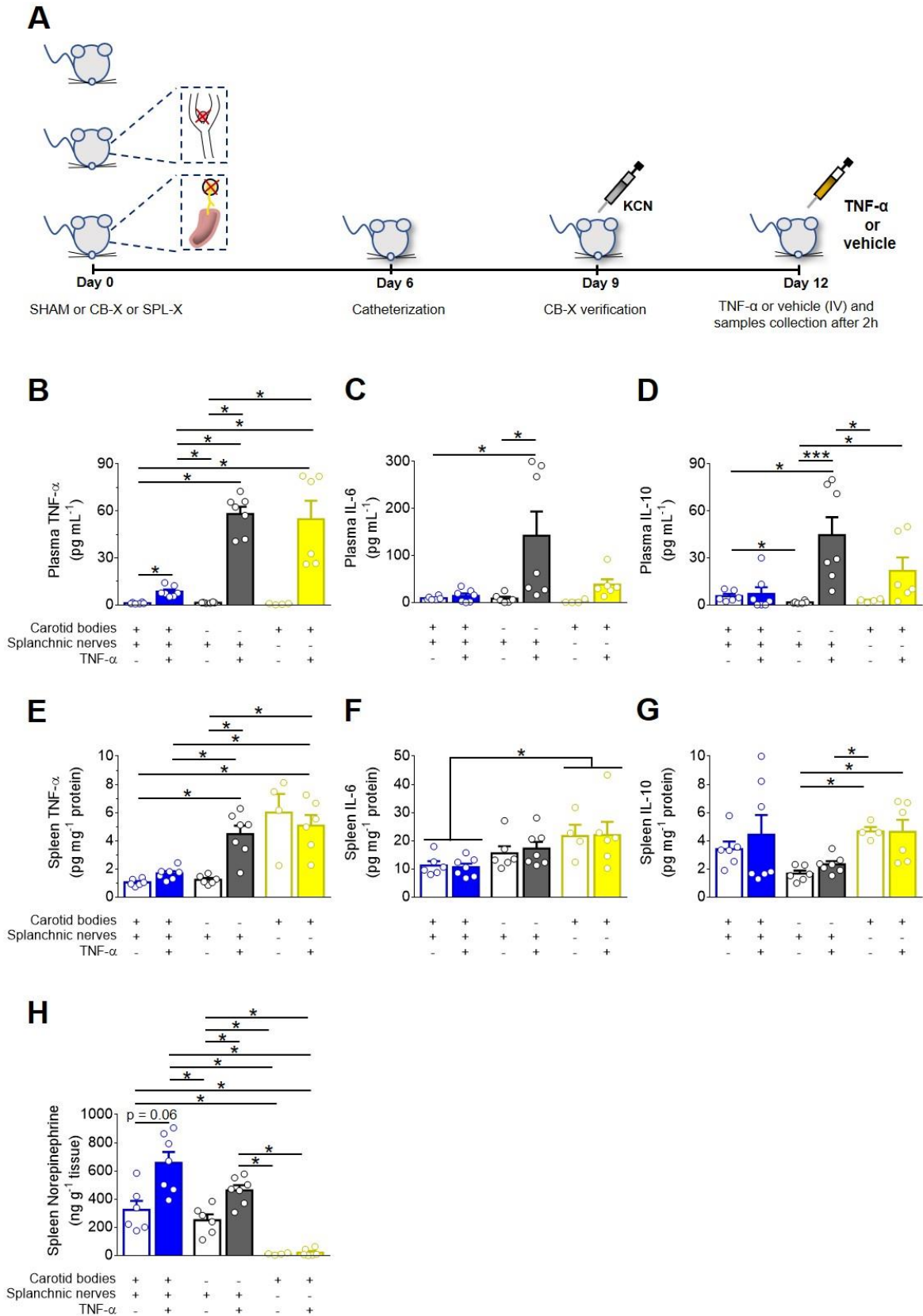
384 **Carotid body ablation or splanchnic sympathetic denervation exacerbates TNF-**  
385  **$\alpha$ -induced inflammation**

386 Considering that the exogenous TNF- $\alpha$  activated a carotid body-cNTS-RVLM circuitry  
387 to excite a specific sympathetic nerve (splanchnic), and because the splanchnic  
388 sympathetic nerves have been considered essential components of sympathetic-  
389 mediated mechanisms to control inflammation (Lankadeva et al., 2020; Martelli et al.,  
390 2014), we next investigated if the activation of this newly described circuit could play  
391 an anti-inflammatory role in the TNF- $\alpha$ -induced inflammation. We found that, in SHAM  
392 rats that received TNF- $\alpha$ , the plasma levels of this cytokine ( $8.5 \pm 1.3$  pg mL<sup>-1</sup>) were  
393 found significantly higher in comparison to SHAM rats that received vehicle ( $1.1 \pm 0.2$   
394 pg mL<sup>-1</sup>) (Figure 5B). It is important to mention that, the half-life of TNF- $\alpha$  is very short  
395 (few minutes) (Ma et al., 2015; Simó et al., 2012), and, hence, it is very likely that the  
396 measured levels of this cytokine in the plasma (2 hours after TNF- $\alpha$  or vehicle  
397 administrations) reflect endogenously produced TNF- $\alpha$ . In rats subjected to either  
398 carotid body ablation (CB-X) or splanchnic sympathetic denervation (SPL-X), the  
399 administration of TNF- $\alpha$  resulted in significant higher plasma levels of this cytokine  
400 compared to SHAM rats injected with TNF- $\alpha$  (CB-X + TNF- $\alpha$  =  $58.1 \pm 4.7$  pg mL<sup>-1</sup>,  
401 SPL-X + TNF- $\alpha$  =  $54.8 \pm 11.8$  pg mL<sup>-1</sup>) (Figure 5B), suggesting that the absence of the  
402 carotid bodies or the splanchnic sympathetic nerves exacerbated the systemic  
403 inflammatory status triggered by the exogenous TNF- $\alpha$ . In the same direction, the  
404 levels of TNF- $\alpha$  in the spleen were found higher in CB-X + TNF- $\alpha$  ( $4.5 \pm 0.6$  pg mg<sup>-1</sup>)  
405 and in SPL-X + TNF- $\alpha$  ( $5.1 \pm 0.8$  pg mg<sup>-1</sup>) groups compared to SHAM + TNF- $\alpha$  ( $1.7 \pm$   
406  $0.2$  pg mg<sup>-1</sup>) group (Figure 5E). These results support the idea that the exogenously  
407 administered TNF- $\alpha$  induced the endogenous production of additional TNF- $\alpha$  likely via  
408 stimulation of splenic macrophages and, that, the removal of the carotid bodies (a  
409 potential sensor of TNF- $\alpha$ ) or of the splanchnic sympathetic nerves (a potential  
410 suppressor of spleen-derived TNF- $\alpha$  production), significantly increased TNF- $\alpha$  levels  
411 in the spleen. It is important to highlight that in SPL-X + vehicle animals, the levels of  
412 TNF- $\alpha$  in the spleen were also elevated ( $6.0 \pm 1.3$  pg mg<sup>-1</sup>) (Figure 5E), reinforcing the  
413 notion that the splanchnic sympathetic innervation of the spleen (via celiac ganglion),  
414 exerts a kind of inhibitory tonus over splenic production of TNF- $\alpha$ . By way of  
415 comparison, in rats with intact splanchnic nerves (SHAM and CB-X) injected with  
416 vehicle, the levels of TNF- $\alpha$  in the spleen were low: (SHAM + vehicle =  $1.0 \pm 0.1$  pg  
417 mg<sup>-1</sup>, CB-X + vehicle =  $1.2 \pm 0.1$  pg mg<sup>-1</sup>) (Figure 5E).



418           Regarding plasma IL-6 levels, CB-X + TNF- $\alpha$  animals displayed higher levels  
419 (142.2  $\pm$  51.0 pg mL<sup>-1</sup>) than SHAM + vehicle (9.1  $\pm$  1.6 pg mL<sup>-1</sup>) and CB-X + vehicle  
420 (8.2  $\pm$  3.8 pg mL<sup>-1</sup>) (Figure 5C). Although not statistically significant, the levels of IL-6  
421 in the plasma tended to be higher in CB-X + TNF- $\alpha$  and SPL-X + TNF- $\alpha$  (38.1  $\pm$  11.2  
422 pg mL<sup>-1</sup>) compared to all other groups: (SHAM + vehicle = 9.1  $\pm$  1.6 pg mL<sup>-1</sup>, SHAM +  
423 TNF-  $\alpha$  = 14.1  $\pm$  5.0 pg mL<sup>-1</sup>, CB-X + vehicle = 8.2  $\pm$  3.8 pg mL<sup>-1</sup>, SPL-X + vehicle =  
424 2.2  $\pm$  1.9 pg mL<sup>-1</sup>) (Figure 5C). Concerning the spleen levels of IL-6, no interactions  
425 between group x treatment were detected by two-way ANOVA. However, a statistically  
426 main effect of group indicated that the spleen levels of IL-6 were higher in SPL-X +  
427 vehicle (21.7  $\pm$  4.0 pg mg<sup>-1</sup>) and SPL-X + TNF- $\alpha$  (22.0  $\pm$  4.7 pg mg<sup>-1</sup>) groups compared  
428 to SHAM + vehicle (11.2  $\pm$  1.5 pg mg<sup>-1</sup>) and SHAM + TNF- $\alpha$  (10.6  $\pm$  1.3 pg mg<sup>-1</sup>)  
429 groups (Figure 5F), suggesting that splanchnic sympathetic denervation was  
430 permissive to IL-6 production in the spleen, even in the absence of the TNF- $\alpha$  stimulus.  
431 With regard to plasma IL-10, the levels of this anti-inflammatory cytokine tended to be  
432 higher in CB-X + TNF- $\alpha$  (44.7  $\pm$  11.4 pg mL<sup>-1</sup>) and SPL-X + TNF- $\alpha$  (21.7  $\pm$  8.6 pg mL<sup>-1</sup>)  
433 <sup>1</sup>) as compared to SHAM + TNF- $\alpha$  (7.1  $\pm$  4.2 pg mL<sup>-1</sup>) and to every other group that  
434 received vehicle (SHAM + vehicle = 5.6  $\pm$  1.4 pg mL<sup>-1</sup>, CB-X + vehicle = 1.7  $\pm$  0.3 pg  
435 mL<sup>-1</sup>, SPL-X + vehicle = 2.8  $\pm$  0.5 pg mL<sup>-1</sup>) (Figure 5D). These results match with the  
436 increased levels of TNF- $\alpha$  in the plasma and the spleen of CB-X and SPL-X rats that  
437 received TNF- $\alpha$ , indicating a worse systemic inflammatory status in these animals.  
438 Finally, spleen levels of IL-10 tended to be lower in both CB-X groups, but was only  
439 statistically different between: CB-X + vehicle (1.7  $\pm$  0.2 pg mg<sup>-1</sup>) compared to SPL-X  
440 + vehicle (4.7  $\pm$  0.3 pg mg<sup>-1</sup>); CB-X + vehicle group compared to SPL-X + TNF- $\alpha$  (4.6  
441  $\pm$  0.9 pg mg<sup>-1</sup>); and between CB-X + TNF- $\alpha$  (2.3  $\pm$  0.2 pg mg<sup>-1</sup>) compared to SPL-X +  
442 vehicle (Figure 5G). In regard to norepinephrine levels in the spleen, SHAM rats  
443 injected with TNF- $\alpha$  displayed the highest mean levels (656.2  $\pm$  77.6 pg mg<sup>-1</sup>), followed  
444 by CB-X + TNF- $\alpha$  (462.3  $\pm$  36.4 pg mg<sup>-1</sup>), SHAM + vehicle (322.9  $\pm$  64.4 pg mg<sup>-1</sup>), CB-  
445 X+ vehicle (249.9  $\pm$  40.9 pg mg<sup>-1</sup>), SPL-X + TNF- $\alpha$  (20.6  $\pm$  10.7 pg mg<sup>-1</sup>), and SPL-X  
446 + vehicle (10.3  $\pm$  3.5 pg mg<sup>-1</sup>) groups (Figure 5H). Note that splanchnic sympathetic  
447 denervation almost depleted the norepinephrine content in the spleen, confirming the  
448 efficacy of the denervation procedure. In addition, the efficacy of splanchnic  
449 sympathetic denervation was also verified by the less pronounced TH staining in the  
450 spleen (figure supplement 4C). The efficacy of the bilateral carotid body ablation  
451 procedure was confirmed by the lack of cardiovascular responses to KCN (figure

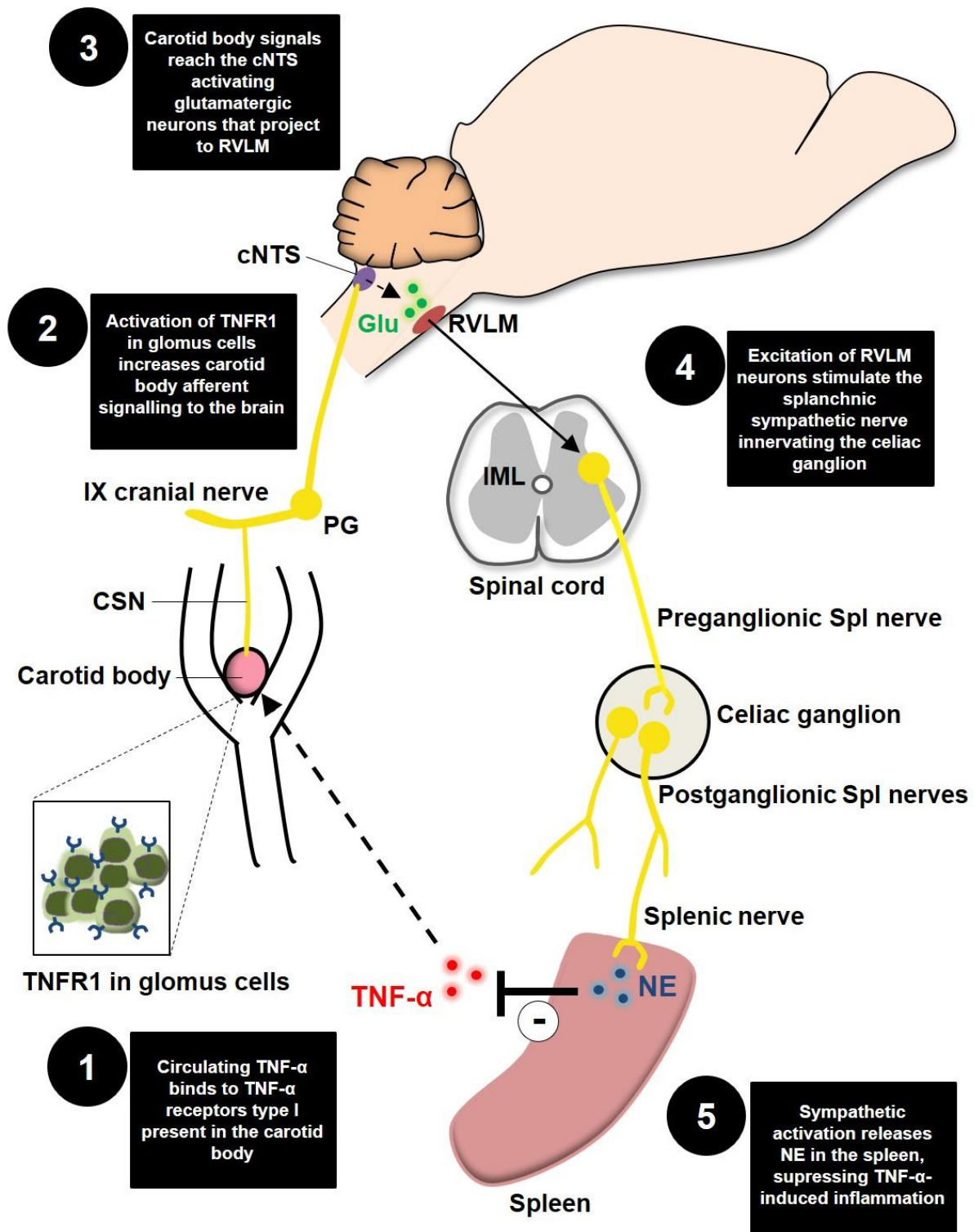
452 supplement 4A – B). Collectively, our data suggest that elevated circulating levels of  
453 TNF- $\alpha$  activates a neural mechanism (carotid body-cNTS-RVLM-splanchnic  
454 sympathetic nerves) that controls the ongoing inflammation by inhibiting the synthesis  
455 of additional TNF- $\alpha$  in the spleen likely via direct norepinephrine-mediated  
456 suppression of splenic macrophage TNF- $\alpha$  production.



457

458 **Figure 5.** Carotid body ablation (CB-X) or splanchnic sympathetic denervation (SPL-X) intensify the  
 459 TNF-α-induced inflammation. **A.** Schematic illustration of the experimental protocol. **B, C and D.**  
 460 Plasma levels of TNF-α, IL-6 and IL-10 in SHAM (blue bars), CB-X (gray bars), and SPL-X (yellow bars)  
 461 rats, measured 2 hours after vehicle (empty bars) or TNF-α (filled bars) intravenous administration (n =  
 462 4 - 7 per group). **B.** Statistically significant differences in the plasma levels of TNF-α across groups were

463 detected:  $H(5) = 31.454$ ,  $p < 0.001$  (Kruskal-Wallis). In SHAM + TNF- $\alpha$ , the plasma levels of this cytokine  
464 were found significantly higher in comparison to SHAM + vehicle ( $U = 0$ ,  $z = -3.000$ ,  $p = 0.001$ , Mann-  
465 Whitney  $U$ -test). In CB-X and SPL-X rats, TNF- $\alpha$  administration resulted in significant higher plasma  
466 levels of this cytokine as compared to SHAM + TNF- $\alpha$ : SHAM + TNF- $\alpha$  vs. CB-X + TNF- $\alpha$  ( $U = 0$ ,  $z = -$   
467  $3.130$ ,  $p = 0.001$ , Mann-Whitney  $U$ -test); SHAM + TNF- $\alpha$  vs. SPL-X + TNF- $\alpha$  ( $U = 0$ ,  $z = -3.000$ ,  $p =$   
468  $0.001$ , Mann-Whitney  $U$ -test). Between vehicle-treated groups, the plasma levels of TNF- $\alpha$  were not  
469 different ( $p > 0.003$ ). Regarding plasma IL-6 levels, significant differences between groups were  
470 detected:  $H(5) = 22.024$ ,  $p = 0.001$  (Kruskal-Wallis). **C.** The plasma levels of IL-6 were higher in CB-X  
471 + TNF- $\alpha$  as compared to SHAM + vehicle ( $U = 1$ ,  $z = -2.857$ ,  $p = 0.002$ , Mann-Whitney  $U$ -test) and to  
472 CB-X + vehicle ( $U = 1$ ,  $z = -2.857$ ,  $p = 0.002$ , Mann-Whitney  $U$ -test). No statistical differences were  
473 found in plasma levels of IL-6 in the other pairwise comparisons ( $p > 0.003$ ). **D.** Finally, the plasma  
474 levels of IL-10 were found significantly different across groups:  $F_{(5, 13.522)} = 14.524$ ,  $p < 0.001$  (Welch  
475 ANOVA). Games-Howell post hoc test revealed that the plasma levels of IL-10 were significantly higher  
476 in CB-X + TNF- $\alpha$  as compared to all groups that received vehicle: CB-X + TNF- $\alpha$  vs. SHAM + vehicle  
477 (Mean difference =  $2.0 \text{ pg mL}^{-1}$ , 95% CI [0.6, 3.3],  $p = 0.005$ ); CB-X + TNF- $\alpha$  vs. CB-X + vehicle (Mean  
478 difference =  $3.1 \text{ pg mL}^{-1}$ , 95% CI [1.8, 4.4],  $p < 0.001$ ); CB-X + TNF- $\alpha$  vs. SPL-X + vehicle (Mean  
479 difference =  $2.6 \text{ pg mL}^{-1}$ , 95% CI [1.2, 3.9],  $p = 0.001$ ). In SPL-X + TNF- $\alpha$ , the plasma levels of IL-10  
480 were higher as compared to CB-X + vehicle (Mean difference =  $2.2 \text{ pg mL}^{-1}$ , 95% CI [0.2, 4.1],  $p =$   
481  $0.032$ ). Between vehicle-administered groups, SHAM rats displayed higher plasma levels of IL10 as  
482 compared to CB-X rats (Mean difference =  $1.2 \text{ pg mL}^{-1}$ , 95% CI [0.1, 2.2],  $p = 0.033$ ). **E, F and G.** Spleen  
483 levels of TNF- $\alpha$ , IL-6 and IL-10 in SHAM (blue bars), CB-X (gray bars), and SPL-X (yellow bars) rats, 2  
484 hours after vehicle (empty bars) or TNF- $\alpha$  (filled bars) intravenous administration ( $n = 4 - 7$  per group).  
485 **E.** Statistically significant differences in the spleen levels of TNF- $\alpha$  between groups were found:  $F_{(5,$   
486  $12.262)} = 12.957$ ,  $p < 0.001$  (Welch ANOVA). Games-Howell post hoc test revealed that the spleen levels  
487 of TNF- $\alpha$  were significantly higher in CB-X and SPL-X that received TNF- $\alpha$  as compared to SHAM rats  
488 that received TNF- $\alpha$ : CB-X + TNF- $\alpha$  vs. SHAM + TNF- $\alpha$  (Mean difference =  $2.8 \text{ pg mg}^{-1}$  protein, 95%  
489 CI [0.5, 5.1],  $p = 0.021$ ); SPL-X + TNF- $\alpha$  vs. SHAM + TNF- $\alpha$  (Mean difference =  $3.4 \text{ pg mg}^{-1}$  protein,  
490 95% CI [0.2, 6.6],  $p = 0.039$ ). Within vehicle-treated groups, the spleen levels of TNF- $\alpha$  were not different  
491 ( $p > 0.05$ ). No statistical differences were found when comparing SHAM + vehicle vs. SHAM + TNF- $\alpha$   
492 (Mean difference =  $-0.6 \text{ pg mg}^{-1}$  protein, 95% CI [-1.3, 0.0],  $p = 0.064$ ). **F.** Regarding the spleen levels  
493 of IL-6, no interactions between group x treatment were detected:  $F_{(2,30)} = 0.092$ ,  $p = 0.912$ , partial  $\eta^2 =$   
494  $0.006$ . However, a statistically significant main effect of group was found:  $F_{(2,30)} = 7.130$ ,  $p = 0.003$ ,  
495 partial  $\eta^2 = 0.322$ . A Bonferroni post hoc analysis indicated that the spleen levels of IL-6 were significant  
496 higher in SPL-X groups as compared to SHAM groups: (Mean difference =  $10.9 \text{ pg mg protein}$ , 95% CI  
497 [3.5, 18.3],  $p = 0.002$ ). **G.** Concerning the spleen levels of IL-10, statistically significant differences  
498 between groups were found:  $F_{(5, 13.792)} = 12.491$ ,  $p < 0.001$  (Welch ANOVA). Games-Howell post hoc  
499 test revealed that the spleen levels of IL-10 were significantly lower in CB-X groups as compared to  
500 SPL-X groups: CB-X + vehicle vs. SPL-X + vehicle (Mean difference =  $-1.1 \text{ pg mg}^{-1}$  protein, 95% CI [-  
501  $1.6, -0.5$ ],  $p = 0.002$ ); CB-X + vehicle vs. SPL-X + TNF- $\alpha$  (Mean difference =  $-1.0 \text{ pg mg}^{-1}$  protein, 95%  
502 CI [-1.8, -0.1],  $p = 0.026$ ); CB-X + TNF- $\alpha$  vs. SPL-X + vehicle (Mean difference =  $-0.7 \text{ pg mg}^{-1}$  protein,  
503 95% CI [-1.1, -0.3],  $p = 0.002$ ). **H.** Spleen levels of norepinephrine in SHAM (blue bars), CB-X (gray  
504 bars), and SPL-X (yellow bars) rats, 2 hours after vehicle (empty bars) or TNF- $\alpha$  (filled bars) intravenous  
505 administration ( $n = 4 - 7$  per group).. Statistically significant differences in the spleen levels of  
506 norepinephrine between groups were found:  $F_{(5, 13.050)} = 45.864$ ,  $p < 0.001$  (Welch ANOVA). \* $p < 0.05$   
507 and \*\*\* $p < 0.001$ . Data are means  $\pm$  SEM. Games-Howell post hoc test revealed that the administration  
508 of TNF- $\alpha$  in SHAM rats, resulted in a trend to increase the spleen norepinephrine levels compared to  
509 SHAM animals receiving vehicle (Mean difference =  $333.3 \text{ pg mg}^{-1}$  tissue, 95% CI [-11.2, 677.8],  $p =$   
510  $0.060$ ) and in significant increases as compared to CB-X + vehicle (Mean difference =  $406.3 \text{ pg mg}^{-1}$   
511 tissue, 95% CI [94.4, 718.2],  $p = 0.011$ ), to SPL-X + vehicle (Mean difference =  $645.9 \text{ pg mg}^{-1}$  tissue,  
512 95% CI [337.1, 954.7],  $p = 0.001$ ), and to SPL-X + TNF- $\alpha$  (Mean difference =  $635.5 \text{ pg mg}^{-1}$  tissue, 95%  
513 CI [327.6, 943.5],  $p = 0.001$ ). In CB-X rats, TNF- $\alpha$  administration led to higher levels of norepinephrine  
514 in the spleen as compared to CB-X + vehicle (Mean difference =  $212.4 \text{ pg mg}^{-1}$  tissue, 95% CI [24.4,  
515  $400.4$ ],  $p = 0.025$ ), to SPL-X + vehicle (Mean difference =  $452.0 \text{ pg mg}^{-1}$  tissue, 95% CI [307.5, 596.6],  
516  $p < 0.001$ ), and to SPL-X + TNF- $\alpha$  (Mean difference =  $441.7 \text{ pg mg}^{-1}$  tissue, 95% CI [298.1, 585.3],  $p <$   
517  $0.001$ ). SPL-X + vehicle animals also displayed lower levels of norepinephrine in the spleen compared  
518 to SHAM + vehicle (Mean difference =  $-312.6 \text{ pg mg}^{-1}$  tissue, 95% CI [-587.0, -38.1],  $p = 0.030$ ) and  
519 CB-X + vehicle (Mean difference =  $-239.6 \text{ pg mg}^{-1}$  tissue, 95% CI [-413.5, -65.7],  $p = 0.013$ ). Similarly,  
520 the levels of norepinephrine in the spleen were also lower in SPL-X + TNF- $\alpha$  compared to SHAM +  
521 vehicle (Mean difference =  $-302.2 \text{ pg mg}^{-1}$  tissue, 95% CI [-574.7, -29.8],  $p = 0.033$ ) and CB-X + vehicle  
522 (Mean difference =  $-229.3 \text{ pg mg}^{-1}$  tissue, 95% CI [-400.7, -57.9],  $p = 0.014$ ).



523  
524  
525  
526  
527  
528  
529  
530  
531

**Figure 6.** Schematic model of the novel proposed neuroimmune mechanism. TNFR1, TNF- $\alpha$  receptors type I; CSN, carotid sinus nerve; IX cranial nerve, glossopharyngeal nerve; PG, petrosal ganglion; cNTS, commissural nucleus tractus solitarius; Glu, glutamate; RLVM, rostral ventrolateral medulla; IML, intermediolateral nucleus; Spl, splanchnic; NE, norepinephrine.



## 532 **Discussion**

533 In the present study, we provide a series of anatomical and functional evidence for the  
534 existence of a previously unrecognized mechanism of neuroimmune interaction. The  
535 main finding is that the carotid body is able to detect elevated levels of the pro-  
536 inflammatory cytokine TNF- $\alpha$  in the blood and communicate with the central nervous  
537 system via carotid sinus nerve afferents, activating RVLM-projecting cNTS excitatory  
538 neurons that contribute to a counteracting sympathetic-mediated anti-inflammatory  
539 response. These results advance our understanding of the complex mechanisms  
540 underlying the bidirectional connection between the nervous and the immune systems.

541 Recently, the carotid bodies emerged as potential candidates for peripheral  
542 detectors of inflammation. This possibility is supported by a growing number of studies  
543 indicating that they are polymodal sensors, able to monitor the chemical composition  
544 of the arterial blood. More specifically, these studies have shown that besides  
545 promoting autonomic and respiratory adjustments in response to arterial hypoxemia  
546 (i.e., peripheral chemoreflex), the carotid bodies can respond to several other  
547 circulating stimuli such as leptin, angiotensin II, glucose, sodium chloride, insulin,  
548 adrenaline, and, also, inflammatory mediators (Allen, 1998; da Silva et al., 2019;  
549 Jendzjowsky et al., 2021, 2018; Katayama, 2016; Kumar and Prabhakar, 2012; Shin  
550 et al., 2019; Thompson et al., 2016). Regarding inflammatory mediators, studies  
551 reported that the carotid body of many species, including rats, cats and humans,  
552 expresses receptors for lysophosphatidic acid (LPA), IL-1 $\beta$ , IL-6, and TNF- $\alpha$   
553 (Fernández et al., 2008; Jendzjowsky et al., 2018; Mkrtchian et al., 2012; Wang et al.,  
554 2002). Accordingly, in the present study, we combined immunofluorescence and  
555 RNAscope FISH protocols to confirm that TNFR1 is expressed in the carotid body of  
556 rats at both mRNA and protein levels. Moreover, in addition to the anatomical  
557 evidence, previous functional studies demonstrated that inflammation-related factors  
558 can impact carotid body activity (Jendzjowsky et al., 2021, 2018; Shu et al., 2007),  
559 opening a wide range of possibilities regarding the role of the carotid body in the  
560 context of neuroimmune interactions. For instance, a recent study showed that LPA  
561 potently increased CSN activity in an isolated perfused carotid body/carotid sinus  
562 nerve preparation (Jendzjowsky et al., 2018). Furthermore, the same research group  
563 showed that the perfusion of the isolated carotid body/carotid sinus nerve preparation  
564 with diverse pro-inflammatory cytokines (IL-4, IL-5, IL-13, IL-1, IL-6, and TNF- $\alpha$ ), one

565 at a time or in combination, also increased CSN activity (Jendzjowsky et al., 2021),  
566 confirming the unique ability of the carotid body to sense and respond to inflammatory  
567 mediators. In our study, CSN activity was recorded in vivo and TNF- $\alpha$  was given  
568 systemically (IV). We chose the IV administration route because it better mimics a real  
569 scenario of systemic inflammation. We observed a progressive and significant  
570 increase in CSN activity, indicating that the carotid body could detect the elevated  
571 levels of TNF- $\alpha$  in the blood and alert the central nervous system via afferent signals.  
572 The reasons by which TNF- $\alpha$  increased CSN activity in a sustained manner (for at  
573 least 2 hours) are not clear, especially because the half-life of TNF- $\alpha$  in the plasma is  
574 reported to be very short (few minutes) (Ma et al., 2015; Simó et al., 2012). We  
575 hypothesize that the exogenous administered TNF- $\alpha$  stimulated the synthesis and  
576 release of additional TNF- $\alpha$ , probably via direct activation of splenic macrophages as  
577 suggested by our data (Figure 5) and/or by indirect activation of liver Kupffer cells as  
578 observed during endotoxemia in rats (Fonseca et al., 2021). This endogenously  
579 produced TNF- $\alpha$  could either sustain the carotid body activation and, also, stimulate  
580 the synthesis of further TNF- $\alpha$ .

581 We found that besides increasing CSN activity, the intravenous administration  
582 of TNF- $\alpha$  promoted the activation of cNTS neurons, the first relay site for carotid body  
583 afferents. Notably, the systemic administration of TNF- $\alpha$  resulted in activation of the  
584 cNTS neurons at the same rostro-caudal levels reported to be activated after carotid  
585 body stimulation by hypoxia or intravenous KCN (Cruz et al., 2010; Kline et al., 2010;  
586 Malheiros-Lima et al., 2020). These cNTS neurons, activated by carotid body  
587 stimulation, project to several brain areas, including the RVLM, to control the  
588 sympathetic nervous system (Kline et al., 2010; Koshiya and Guyenet, 1996). A  
589 previous study observed that after 3 hours of hypoxia (10% O<sub>2</sub>) exposure, a high  
590 proportion of RVLM-projecting cNTS neurons were activated (Kline et al., 2010).  
591 Furthermore, the authors injected anterograde tracers into the carotid body and  
592 observed that carotid body afferents terminate in close apposition to the RVLM-  
593 projecting cNTS neurons. Thus, this neural circuitry elegantly revealed by Kline et al.  
594 (2010), along with previous data (Aicher et al., 1996; Koshiya and Guyenet, 1996),  
595 provides a major neural pathway for hypoxia-induced sympathoexcitation. Of note, the  
596 blockade of glutamatergic receptors in the NTS was shown to strongly reduce the  
597 sympathetic responses to chemical stimulation of the carotid body (Ferreira et al.,  
598 2018). Since in the present study, circulating TNF- $\alpha$  induced the activation of RLVM-



599 projecting cNTS glutamatergic neurons at the same rostro-caudal levels reported in  
600 the literature (Cruz et al., 2010; Kline et al., 2010; Malheiros-Lima et al., 2020) and,  
601 because carotid body ablation almost abolished the activation of these neurons, we  
602 believe that TNF- $\alpha$  might be stimulating a similar neural pathway (carotid body-cNTS-  
603 RVLM) activated by hypoxia to increase sympathetic activity. It is important to highlight  
604 that more than a half of c-FOS positive neurons observed in SHAM rats treated with  
605 TNF- $\alpha$  were not co-localized with FG (non-RVLM-projecting). We hypothesize that  
606 these neurons project to other nuclei involved in sympathetic modulation, such as the  
607 PVN, regions involved in respiratory control, and vagal nuclei (Luise King et al., 2012;  
608 Malheiros-Lima et al., 2020; Neff et al., 1998; Willis et al., 1996; Zera et al., 2019). In  
609 fact, recent studies suggested that inflammation-induced carotid body stimulation  
610 could also activate brainstem vagal nuclei (nucleus ambiguus and dorsal motor  
611 nucleus of the vagus) to increase parasympathetic activity (Jendzjowsky et al., 2021,  
612 2018). Therefore, the results of the present and previous studies suggest that the  
613 carotid body detects circulating inflammatory mediators and activates central  
614 autonomic areas to modulate sympathetic and/or parasympathetic functions.

615 Our study shows that the TNF- $\alpha$ -induced activation of a sympathoexcitatory  
616 circuit (carotid body-cNTS-RVLM) resulted in increased SNA as revealed by  
617 simultaneous recordings of splanchnic, renal and lumbar SNA. To the best of our  
618 knowledge, this is the first study describing the effects of circulating TNF- $\alpha$ , an  
619 important inflammatory mediator, on the activity of three different sympathetic nerves  
620 recorded simultaneously in vivo. Previous studies have already demonstrated that  
621 circulating TNF- $\alpha$  increases renal SNA in rats (Wei et al., 2013; Zhang et al., 2003).  
622 However, since sympathetic outflows to other tissues/organs have distinct functions  
623 and can be differentially regulated (Morrison, 2001; Tromp et al., 2018), it becomes  
624 relevant to study the effects of TNF- $\alpha$  on sympathetic outflows directed to other targets  
625 besides the kidneys. Here, we found that TNF- $\alpha$  promoted a generalized activation of  
626 the sympathetic nervous system, increasing splanchnic, renal, and lumbar SNA in  
627 carotid body-intact rats. The removal of the afferent inputs from the carotid bodies (by  
628 bilateral carotid body ablation) blunted, in part, this TNF- $\alpha$ -induced sympathetic  
629 activation, consistent with the attenuated activation of RLVM-projecting cNTS neurons  
630 observed in CB-X rats (Figure 3C – E). Interestingly, the blunting effect of carotid body  
631 ablation was significant only on splanchnic SNA. Therefore, our data indicate that  
632 increased circulating TNF- $\alpha$  activates a carotid body-cNTS-RVLM neural circuit that

633 selectively controls splanchnic SNA in this condition. It is noteworthy that a previous  
634 study reported that the increase in renal SNA following the systemic administration of  
635 TNF- $\alpha$  was largely attenuated in rats with lesions of the subfornical organ (Wei et al.,  
636 2013). It suggests that splanchnic, renal, and lumbar SNA might be under the control  
637 of different neural routes and might have different functions in the course of TNF- $\alpha$ -  
638 driven inflammation.

639 In this context, some studies have suggested that the splanchnic sympathetic  
640 nerves play an important immunomodulatory role during endotoxemia-induced  
641 systemic inflammation (Lankadeva et al., 2020; Martelli et al., 2014). For instance, it  
642 was demonstrated that acute endotoxemia induced by intravenous administration of  
643 lipopolysaccharide (LPS) significantly increased plasma levels of TNF- $\alpha$  after 90  
644 minutes in rats (Martelli et al., 2014). In parallel, this LPS administration potently  
645 increased splanchnic SNA. Notably, when LPS was given to rats subjected to the  
646 bilateral section of the splanchnic sympathetic nerves, the plasma TNF- $\alpha$  levels  
647 increased 5 times more than those of intact rats (Martelli et al., 2014). Together, these  
648 results indicate that during LPS-induced systemic inflammation, the splanchnic SNA  
649 increases to counteract the ongoing inflammation in a kind of negative feedback reflex.  
650 Since, in the present study, the elevated circulating TNF- $\alpha$  activated a carotid body-  
651 cNTS-RVLM neural circuit to increase splanchnic SNA, we hypothesized that this  
652 mechanism could be a neuroimmune reflex to counteract the TNF- $\alpha$ -induced  
653 inflammation. To test this hypothesis, we removed either the detection/afferent arm  
654 (i.e., the carotid bodies) or the efferent arm (i.e., the splanchnic sympathetic nerves)  
655 of this potential neuroimmune reflex and subjected these animals (and SHAM control  
656 animals) to systemic injections of TNF- $\alpha$  or vehicle. After 2 hours, we quantified the  
657 levels of TNF- $\alpha$ , IL-6, and IL-10 in the blood and in the spleen as well as the levels of  
658 norepinephrine in the spleen. We found that in SHAM rats, the administration of TNF-  
659  $\alpha$  significantly increased the plasma levels of TNF- $\alpha$  and slightly increased the spleen  
660 levels of TNF- $\alpha$  compared to vehicle-injected SHAM rats. In addition, TNF- $\alpha$   
661 administration tended to increase spleen norepinephrine levels in SHAM animals as  
662 compared to its vehicle-treated counterparts (Figure 5H,  $p = 0.06$ ), consistent with our  
663 data showing a TNF- $\alpha$  induced splanchnic SNA activation. Interestingly, in rats  
664 subjected to either carotid body ablation or splanchnic sympathetic denervation, the  
665 administration of TNF- $\alpha$  resulted in exacerbated levels of pro-inflammatory cytokines  
666 in the plasma and the spleen, supporting the idea that both the detection/afferent arm

667 and the efferent arm are important components of a neuroimmune regulatory  
668 mechanism that detects and modulates acute inflammation through sympathetic  
669 activation towards the spleen. Disrupting the afferent/detection component (carotid  
670 body ablation) resulted in a peculiar elevation of all quantified cytokines, including IL-  
671 10 (an anti-inflammatory cytokine). The reason for this elevation in plasma IL-10 in  
672 CB-X rats treated with TNF- $\alpha$  is not clear. This could result from the fact that carotid  
673 body ablation eliminated only part of the autonomic circuits toward the spleen, possible  
674 preserving and/or amplifying other counter-inflammatory mechanisms. In fact, the  
675 administration of TNF- $\alpha$  in CB-X rats, still activated splanchnic SNA and resulted in a  
676 significant increase in splenic levels of norepinephrine compared to vehicle-injected  
677 CB-X rats. However, the TNF- $\alpha$ -induced splanchnic SNA activation and  
678 norepinephrine release in the spleen were attenuated in CB-X rats compared to SHAM  
679 rats, which could explain, at least in part, the exacerbated inflammatory status  
680 observed in the animals lacking the carotid bodies. Differently, the interruption of the  
681 efferent component (splanchnic sympathetic denervation) completely blocked the  
682 sympathetic signalling to the spleen, removing the norepinephrine “inhibitory tonus”  
683 on cytokine production by splenic macrophages, resulting in elevated splenic cytokine  
684 levels even in those animals administered with saline. Collectively, our data suggest  
685 the existence of an intrinsic and physiological anti-inflammatory reflex that depends  
686 on a detection/afferent arm (i.e., the carotid bodies and the carotid sinus nerve), on a  
687 central integrative pathway (i.e., RVLM-projecting cNTS neurons), and on an  
688 effector/efferent arm (i.e., splanchnic sympathetic nerves) that modulates the splenic  
689 production of cytokines through norepinephrine release.

690 The findings of the present study are novel and place the carotid body as a  
691 critical player in the context of neuroimmune interactions. In the last years, the  
692 contribution of the carotid bodies to sympathetic overactivity has been implicated in  
693 the pathophysiology of several diseases such as sleep apnoea, hypertension, and  
694 heart failure (Marcus et al., 2014; McBryde et al., 2013; Melo et al., 2019; Narkiewicz  
695 et al., 2016; Niewinski et al., 2017; Yuan et al., 2016). In these conditions, exaggerated  
696 tonic CSN activity leads to chronic activation of the sympathetic nervous system, often  
697 associated with a poor prognosis. Here, we found that the acute carotid body-mediated  
698 sympathetic activation induced by intravenous TNF- $\alpha$  is likely to be beneficial because  
699 it exerted a counteracting anti-inflammatory reflex. However, it is possible that in  
700 chronic pathological inflammatory conditions, the long-term activation of this carotid

701 body-dependent neuroimmune circuit leads to side effects because it generates an  
702 aberrant tonic CSN input to central sympathetic networks, leading to sustained  
703 sympathetic overactivity to multiple target organs. This possibility raises an intriguing  
704 question on whether circulating inflammatory factors could trigger the carotid body-  
705 mediated sympathetic overactivity observed in diseases such as hypertension  
706 (McBryde et al., 2013; Narkiewicz et al., 2016) and heart failure (Marcus et al., 2014;  
707 Niewinski et al., 2017) since these conditions are associated with increased systemic  
708 inflammation (Bautista et al., 2005; Norlander et al., 2018; Rauchhaus et al., 2000;  
709 Sesso et al., 2015). On the other hand, defects in the carotid body-mediated  
710 neuroimmune reflex described here, could impair the ability to regulate the levels of  
711 inflammatory mediators in the bloodstream, amplifying systemic inflammation.  
712 Nevertheless, further investigations are needed to clarify the beneficial or detrimental  
713 effects following the activation/inactivation of the neuroimmune mechanism described  
714 in the present study under different conditions and to explore its therapeutic potential  
715 in the treatment of inflammatory diseases.

716

717

## 718 **Methods**

### 719 **Animals and ethical approval**

720 All experimental procedures were reviewed and approved by the Ethical Committee in  
721 Animal Experimentation of the Araraquara School of Dentistry, São Paulo State  
722 University (protocol nº 17/2019) and conducted following the Guide for the Care and  
723 Use of Laboratory Animals from the Brazilian National Council for Animal  
724 Experimentation Control. Experiments were performed on adult male *Holtzman* rats  
725 (320 - 400 g) obtained from the Animal Care Unit of the São Paulo State University  
726 (Araraquara, SP, Brazil). The animals were housed in collective cages (2 - 4  
727 animals/cage), provided with chow and water *ad libitum*, and maintained under  
728 controlled conditions of temperature ( $22 \pm 1^\circ\text{C}$ ), humidity (50 - 60%) in a 12:12 hours  
729 light/dark cycle.

730

731

732

733

734 **General procedures**

735 All surgical procedures were performed under aseptic conditions. The appropriate  
736 depth of anesthesia was confirmed by the absence of withdrawal reflex and corneal  
737 reflexes in response to pinching the toe. Throughout the surgical procedures and the  
738 experimental protocols performed under anesthesia (described below), the body  
739 temperature was measured by a rectal probe and maintained at  $37 \pm 0.5^{\circ}\text{C}$  with a  
740 water-circulating heating pad.

741

742

743 **Experiment 1: Expression of TNF- $\alpha$  receptor type I in carotid body glomus cells**

744 Rats were deeply anesthetized with isoflurane (5% in 100 O<sub>2</sub>) and subjected to  
745 transcardial perfusion with cold phosphate-buffered saline (PBS, 10 mM, pH 7.4, 100  
746 mL/100 g BW) followed by paraformaldehyde (PFA, 4% in PBS, 100 mL/100 g BW).  
747 Whole carotid bifurcations containing the carotid bodies were collected as previously  
748 described (Pijacka et al., 2018) and fixed in PFA for 24 hours at 4<sup>o</sup> C. Next, carotid  
749 bifurcations were transferred to 10% sucrose solution and kept at 4<sup>o</sup> C until the tissue  
750 sinks. This procedure was repeated with 20% and 30% sucrose solutions. Carotid  
751 bifurcations were frozen in Tissue Freezing Medium (Triangle Biomedical Sciences,  
752 Durham, NC, USA) using dry ice, sectioned at 10  $\mu\text{m}$  in a cryostat and mounted on  
753 microscope slides (Superfrost Plus, Fisher Scientific, Pittsburgh, PA, USA). To  
754 evaluate the expression of TNF- $\alpha$  receptor type I (TNFR1) in the carotid bodies, we  
755 employed two different approaches: 1) a fluorescent *in situ hybridization* (FISH) assay  
756 (RNAscope, Advanced Cell Diagnostics, Newark, CA, USA) for TNFR1 mRNA  
757 detection combined with immunofluorescence staining for TH (a marker of carotid  
758 body glomus cells) and; 2) a double immunofluorescence staining for TNFR1 and TH.  
759 In the first approach, the FISH assay was performed according to the manufacturer  
760 instructions (document #323100-USM, available at  
761 <https://acdbio.com/documents/product-documents>) and the following materials were  
762 used: RNAscope Multiplex Fluorescent Detection Reagents v2 (product #323110), the  
763 kit RNAscope H<sub>2</sub>O<sub>2</sub> and Protease Reagents (product #322381), the RNAscope probe  
764 for TNFR1 (product #408111) and the TSA Cyanine 3 Plus Evaluation kit (product  
765 #NEL744001KT, Akoya Biosciences, Boston, MA, USA). After completing the FISH  
766 protocol, an immunofluorescence protocol for TH was performed to identify carotid  
767 body glomus cells. Briefly, the slides were incubated in a blocking solution (0.1 M PBS,

768 10% normal horse serum, and 0.3% Triton X-100) for 20 min and subsequently rinsed  
769 3 x 10 minutes in 0.1 M PBS at room temperature. Then, the slides were incubated in  
770 primary antibody (Mouse anti-TH antibody, 1:1000, product #MAB5280, Millipore,  
771 Billerica, MA, USA) for 1 hour at room temperature and 36 hours at 4° C. After rinsing  
772 in PBS, the slides were incubated in secondary antibody (Alexa Fluor 488 donkey anti-  
773 mouse antibody, 1:200, product #R37114, Molecular Probes-Life Technologies,  
774 Eugene, OR, USA) for 4 hours at room temperature. The slides were rinsed in PBS,  
775 the excess liquid was drained, mounting medium (Fluoromount) was dropped on the  
776 tissue and slides were covered with glass coverslips (Fisherfinest). In the second  
777 approach, the immunofluorescence staining as carried out as described above but  
778 adding also a primary antibody for TNFR1 (Rabbit anti-TNFR1, 1:500, product  
779 #ab19139, Abcam, Cambridge, MA, USA) and a secondary antibody (Alexa Fluor 594  
780 donkey anti-rabbit antibody, 1:200, product #A21207, Molecular Probes-Life  
781 Technologies). Images were acquired using a laser scanning confocal microscope  
782 (LSM800, Zeiss). For presentation purposes (color-blind safe) images were pseudo-  
783 colored and representative figures were prepared using the Zen 2 software (Blue  
784 edition, Zeiss).

785

786

## 787 **Experiment 2: Effects of circulating TNF- $\alpha$ on carotid sinus nerve afferent** 788 **activity**

789 Animals were anesthetized with isoflurane (Induction 5% and maintenance 2.5% in  
790 100% O<sub>2</sub>) and subjected to femoral artery and vein catheterizations for arterial blood  
791 pressure (ABP) monitoring and drug administration, respectively, using polyethylene  
792 catheters (PE-50 attached to PE-10, Becton Dickinson, Sparks, MD, USA). Next,  
793 through a midline neck incision, the trachea was cannulated, and animals were  
794 artificially ventilated with a rodent ventilator (model 7025, Ugo Basile, Gemonio, VA,  
795 Italy). End-tidal CO<sub>2</sub> was maintained between 4 - 5% (Capstar-100 carbon dioxide  
796 analyzer, CWE, Ardmore, PA, USA) by adjusting tidal volume (0.7 - 0.8 mL/100 g of  
797 body weight) and respiratory rate (60 - 80 bpm). Isoflurane was slowly replaced with  
798 urethane anesthesia (1.2 - 1.4 g/kg of body weight, IV) given over 20 - 25 minutes.  
799 Then, O<sub>2</sub> concentration in ventilated air was switched to 50% O<sub>2</sub> (balance N<sub>2</sub>) and this  
800 condition was kept until the end of the experiments. This slightly hyperoxic



801 concentration was chosen because it ensures a stable preparation without silencing  
802 carotid body activity as 100% O<sub>2</sub> would do (Kim et al., 2018; Schultz et al., 2007) and  
803 to avoid any period of hypoxia during the experimental protocol.

804 Then, animals were prepared for recordings of CSN afferent activity. The left  
805 carotid sinus nerve was identified, carefully isolated, and cut centrally at its junction to  
806 the glossopharyngeal nerve. CSN activity was recorded using bipolar suction  
807 electrodes and signals were filtered (100 - 3000 Hz), amplified (10,000 X) and digitally  
808 sampled (10 kHz). After baseline recordings, TNF- $\alpha$  (500 ng in 0.5 mL sterile saline,  
809 IV; PeproTech, Rocky Hill, NJ, USA) was administered and CSN activity was recorded  
810 for additional 2 hours. This dose was chosen based on previous works studying the  
811 effects of TNF- $\alpha$  on renal SNA in vivo (Zhang et al. 2003, Wei et al. 2015). Reliability  
812 of CSN activity was confirmed at the end of experiments by a robust increase in  
813 electrical activity during the exposure to hypoxia (10% O<sub>2</sub>) for 60 - 90 seconds.

814

815

### 816 **Experiment 3: Neuroanatomical identification of carotid body-related central** 817 **sympathoexcitatory pathways activated by circulating TNF- $\alpha$**

818 First, the animals were anesthetized with a mixture of ketamine (80 mg kg<sup>-1</sup>, IP; União  
819 Química Farmacêutica Nacional S/A, Embu-Guaçu, SP, Brazil) and xylazine (8 mg kg<sup>-1</sup>,  
820 IP; Hertape Calier Saúde animal S/A, Juatuba, MG, Brazil), and placed in a  
821 stereotaxic frame (David Kopf instruments, Tujunga, CA, USA). The retrograde tracer  
822 FluoroGold (FG, 2%, Fluorochrome, Denver, CO, USA) diluted in artificial  
823 cerebrospinal fluid (aCSF) was then bilaterally injected (40 nL) into the RVLM.  
824 Microinjections were performed with a pressure microinjector (Picospritzer III, Parker  
825 Hannifin, Hollis, NH, USA) using glass micropipettes. After each injection, the  
826 micropipette was kept in place for 2 minutes to prevent FG reflux. The coordinates  
827 used to target the RVLM were: 3.5 mm caudal from Lambda, 1.8 - 2.0 mm lateral from  
828 the midline, and 9.4 mm ventral from the skull surface. After injections, the skin  
829 incisions were sutured and the animals received anti-inflammatory ketoprofen (3 mg  
830 kg<sup>-1</sup>, SC) and antibiotics penicillin (50,000 IU, IM). This treatment was repeated every  
831 24 hours for 3 days.

832 After 6 days recovery, animals were subjected to bilateral carotid body ablation  
833 (CB-X group) or Sham procedure (Sham group) and femoral artery/vein  
834 catheterizations. Carotid body ablation was performed by combining two previously



835 described methods (Katayama et al., 2015; Pijacka et al., 2018). Briefly, animals were  
836 anesthetized with ketamine/xylazine as previously described. The carotid body  
837 arteries were ligated and cut, followed by surgical removal of the carotid bodies on  
838 both sides. In this procedure, the carotid sinus nerve is maintained intact, preserving  
839 carotid baroreflex function (Pijacka et al., 2018). Sham procedure consisted in isolation  
840 of carotid body arteries and carotid bodies, but these structures were kept intact. Neck  
841 incisions were closed with sutures. Femoral artery/vein catheters were tunneled  
842 subcutaneously, exteriorized and fixed in the interscapular region as previously  
843 described (Katayama et al., 2019). After surgeries, animals were treated with  
844 antibiotics and anti-inflammatory for 3 days as described before. To maintain catheters  
845 patency, arterial and venous catheters were flushed every day with heparinized saline  
846 (arterial: 500 U/mL, venous: 40 U/mL). Three days after surgery, ABP was recorded  
847 in unanesthetized rats under baseline conditions and in response to potassium  
848 cyanide (KCN; 40 ug/animal, IV) to verify the efficacy of carotid body ablation in CB-X  
849 group and the integrity of carotid bodies in SHAM group. Successful bilateral carotid  
850 body ablation was confirmed by the lack of cardiovascular responses to KCN (figure  
851 supplement 2A – B). Rats were allowed to recover for 3 days before the next  
852 experimental protocol.

853 On the day of the experiment (12 days after FG microinjections), rats were  
854 administered with TNF- $\alpha$  (500 ng in 0.5 mL sterile saline, IV) and left undisturbed for  
855 2 hours. Next, rats were deeply anesthetized with urethane (IV) and transcardially  
856 perfused with PBS followed by PFA. Brains were collected and fixed in PFA for 12  
857 hours at 4<sup>o</sup> C. Brains were then transferred to 20% sucrose solution and maintained  
858 at 4<sup>o</sup> C until the tissue sinks. Finally, brains were frozen in Tissue Freezing Medium  
859 (Triangle Biomedical Sciences, Durham, NC, USA) and coronal brain slices (30  $\mu$ m)  
860 containing the cNTS and the RVLM were obtained on a cryostat. The RVLM sections  
861 were mounted on microscope slides (Superfrost Plus, Fisher Scientific, Pittsburgh, PA,  
862 USA) and used to confirm the location of FluoroGold microinjections within RVLM  
863 region (From 12.48 mm to 12.00 mm caudal to bregma, ventral to the compact  
864 formation of the Nucleus Ambiguus) accordingly to the rat brain in stereotaxic  
865 coordinates atlas (Paxinos and Charles Watson, 2007). The cNTS sections were  
866 stored in cryoprotectant solution at -20<sup>o</sup> C until processing for c-FOS and VGlut2  
867 immunofluorescence as described below.

868 Briefly, sections were first rinsed in 0.1 M PBS for 10 minutes followed by  
869 incubation in blocking solution (0.1 M PBS, 10% normal horse serum, and 0.3% Triton  
870 X-100) for 20 min at room temperature. After rinsing 3 x 10 minutes in 0.1 M PBS at  
871 room temperature, slides were incubated in primary antibodies for c-FOS (1:1000,  
872 rabbit anti-c-FOS polyclonal antibody, product #sc-52, Santa Cruz Biotechnology,  
873 Santa Cruz, CA, USA) and for VGluT2 (1:2000, guinea pig anti-VGluT2 polyclonal  
874 antibody, product #AB2251-I, Millipore, Temecula, CA, USA) for 1 hour at room  
875 temperature plus 36 hours at 4<sup>o</sup> C. After rinsing in PBS, slides were incubated in  
876 secondary antibodies against rabbit (1:400, donkey anti-rabbit Alexa Fluor 594,  
877 product #A-21207, Molecular Probes-Life Technologies, Eugene, OR, USA) and  
878 against anti-guinea pig (1:400, donkey anti-guinea pig Alexa Fluor 488, product #706-  
879 545-148, Jackson ImmunoResearch Inc, West Grove, PA, USA) for 4 hours at room  
880 temperature. Slides were rinsed in PBS, the excess liquid was drained, mounting  
881 medium (Fluoromount, product # F4680, Sigma, St. Louis, MO, USA) was dropped on  
882 the tissue and slides were covered with glass coverslips (Fisherfinest, product  
883 #125485M, Fisher Scientific).

884 Images were acquired using a laser scanning confocal microscope (LSM800  
885 with airyscan, Zeiss, Jena, TH, Germany). Quantification of retrograde labeled FG  
886 cells, c-FOS positive cells, FG/c-FOS cells, and FG/c-FOS/VGluT2 cells within the  
887 cNTS were performed on brainstem sections from three different rostro-caudal levels  
888 (between 14.76 mm to 14.04 mm caudal to bregma). These levels were chosen based  
889 on studies demonstrating NTS regions that are activated after carotid body stimulation  
890 (Cruz et al., 2010; Kline et al., 2010; Malheiros-Lima et al., 2020). As anatomical  
891 landmarks to identify the cNTS levels, we used: the area postrema, the central canal,  
892 the gracile nucleus, and the hypoglossal nucleus. Cell counting was performed on  
893 ImageJ software (U.S. National Institutes of Health, Bethesda, MD, USA) and  
894 representative figures were prepared using the Zen 2 software (Blue edition, Zeiss).

895

896

#### 897 **Experiment 4: Sympathetic responses to circulating TNF- $\alpha$ in Sham and carotid** 898 **body-ablated (CB-X) rats**

899 Animals were anesthetized, subjected to femoral artery/vein catheterizations,  
900 tracheotomized and continuously ventilated with 50% O<sub>2</sub> (balance N<sub>2</sub>) as described in

901 *Experiment 2.* Next, animals were subjected to bilateral carotid body ablation or sham  
902 surgery as described in *Experiment 3*. All animals were then prepared for  
903 simultaneous recordings of lumbar, renal, and splanchnic sympathetic nerve activity  
904 (SNA). Lumbar sympathetic nerve was isolated through a midline laparotomy and  
905 retraction of vena cava, while renal and splanchnic sympathetic nerves were isolated  
906 through a retroperitoneal incision and careful retraction of the left kidney. Each  
907 sympathetic nerve was placed on a bipolar stainless-steel electrode and insulated with  
908 KWIK-SIL (World Precision Instruments, Sarasota, FL, USA). The raw SNA signals  
909 were filtered (100 - 1000 Hz), amplified (10,000 X) using biological amplifiers (P511  
910 AC Amplifier, Grass Technologies, Warwick, RI, USA), displayed on oscilloscopes  
911 (TDS 2022, Tektronix, Beaverton, OR, USA) and digitally sampled (2 kHz) by a data  
912 acquisition system (Micro 1401, Cambridge Electronic Design Limited). All incisions  
913 were closed with surgical clips (Fine Science Tools, Foster City, CA, USA).

914 After stabilization (~30 minutes after the end of surgical procedures), baseline  
915 recordings of ABP, lumbar, renal and splanchnic SNA were performed. Next, TNF- $\alpha$   
916 (500 ng in 0.5 mL sterile saline, IV) was administered and ABP and SNA were  
917 recorded for additional 2 hours. At the end of the experiments, carotid body ablation  
918 was confirmed by the absence of blood pressure and SNA responses to KCN (40  
919 ug/animal, IV) and these results are presented in figure supplement 3A – B.

920

921

## 922 **Experiment 5: Plasma and spleen levels of pro-inflammatory cytokines following** 923 **intravenous TNF- $\alpha$ in SHAM, CB-X and SPL-X rats**

924 Rats were anesthetized with ketamine/xylazine and prepared accordingly one of the  
925 following experimental groups: 1) CB-X: Animals were subjected to bilateral ablation  
926 of the carotid bodies; 2) SPL-X: Animals were subjected to splanchnic denervation  
927 through celiac ganglionectomy as previously reported in the literature (Asirvatham-  
928 Jeyaraj et al., 2021; Li et al., 2010). Briefly, after a midline laparotomy, the visceral  
929 organs were gently retracted, and the celiac ganglion was localized and surgically  
930 removed using blunt forceps. 3) SHAM: The carotid bodies and the celiac ganglion  
931 were localized and manipulated, but these structures were kept intact. All animals  
932 were allowed to recover for 6 days. Next, animals were subjected to femoral  
933 artery/vein catheterizations. The efficacy of carotid body ablation in CB-X group and  
934 the integrity of carotid bodies in SHAM and SPL-X groups was verified three days after

935 catheterizations and these results are presented in figure supplement 4A – B. Then,  
936 rats were allowed to recover for additional 3 days before the experimental protocol.

937 The experimental protocol consisted in the administration of TNF- $\alpha$  (500 ng, IV)  
938 or vehicle (sterile saline, IV) in SHAM, CB-X and SPL-X rats. After 2 hours, rats were  
939 deeply anesthetized for tissue collection. Blood was collected into EDTA-containing  
940 tubes, centrifuged (1500 rpm for 10 min) at 4° C and the plasma was aliquoted and  
941 stored at -80° C. Spleen was harvested, flash frozen using liquid nitrogen and stored  
942 at -80° C.

943 The spleen samples were homogenized in PBS using a Polytron tissue  
944 homogenizer, and then centrifuged at 10,000 rpm for 2 min at 4 °C. The plasma and  
945 splenic levels of cytokines were quantified by enzyme-linked immunosorbent assay  
946 (ELISA) using commercial kits DuoSet ELISA Development Systems (R&D Systems,  
947 Minneapolis, MN, USA) for TNF- $\alpha$  (catalog #DY510), IL-6 (catalog #DY506), and IL-  
948 10 (catalog #DY522) and following the user manual instructions. The results were  
949 expressed as cytokine concentration in pg/mL and pg/mg of protein, based on  
950 standard curves, respectively. Spleen norepinephrine was measured as previously  
951 described (Garofalo et al., 1996) using HPLC (LC20AT-Shimadzu Proeminence)  
952 coupled to an electrochemical detector (Decade Lite-Antec Scientific) with a 5- $\mu$ m  
953 Spherisorb ODS-2 reversed-phase column (Sigma-Aldrich) and the results were  
954 expressed as norepinephrine concentration in ng/g of tissue.

955

956

### 957 **Statistical analysis**

958 All statistical analyses were performed using IBM SPSS Statistics (version 25, IBM  
959 corporation). Data are reported as means  $\pm$  SEM. The significance level was set at p  
960 < 0.05, unless otherwise stated. No outliers were found as assessed by boxplot  
961 analyses. *Experiment 2:* To examine differences between means within the same  
962 group over time, the one-way repeated measures analysis of variance (ANOVA)  
963 followed by post hoc analysis with Bonferroni adjustment was performed. The normal  
964 distribution of the data was verified and confirmed by the Shapiro-Wilk test, and the  
965 Mauchly's test indicated that the assumption of sphericity has not been violated.  
966 *Experiment 3:* To determine differences between two groups at a single time-point, we  
967 first assessed the distribution of the data using the Shapiro-Wilk test and the  
968 homogeneity of variances using the Levene's test. For normally distributed data with

969 homogenous variances, an unpaired two-tailed Student's *t*-test was performed. In  
970 cases in which the data was normally distributed but the assumption of homogeneity  
971 of variances was violated, an unpaired two-tailed Welch's *t*-test was used. When data  
972 was not normally distributed, an unpaired two-tailed Mann-Whitney *U*-test was applied.  
973 *Experiment 4:* To determine group x time interactions, a two-way repeated measures  
974 ANOVA was conducted. In this case, the normal distribution of the studentized  
975 residuals was verified and confirmed by the Shapiro-Wilk test. The sphericity for the  
976 interaction term was assessed by the Mauchly's test. When the assumption of  
977 sphericity was violated, the Greenhouse-Geisser correction was used and the  
978 estimated epsilon ( $\epsilon$ ) value was reported. Once statistically significant group x time  
979 interactions were detected, simple main effects of group were analyzed using repeated  
980 measures general linear models with Bonferroni adjustment. *Experiment 5:* To  
981 examine group x treatment interactions and main effects of group, a two-way ANOVA  
982 with Bonferroni post hoc was performed. The distribution of the residuals was  
983 examined by the Shapiro-Wilk test. The homoscedasticity was analyzed by the  
984 Levene's test and by plotting the residuals against the predicted values in a simple  
985 scatterplot. If the assumptions of normal distribution and/or homoscedasticity were  
986 violated, the dependent variable was log-transformed when appropriate. When both  
987 the assumptions of normality and homoscedasticity (requirements for two-way  
988 ANOVA) were not satisfied even after transformation, a Kruskal-Wallis followed by  
989 Mann-Whitney *U*-tests for pairwise comparisons between groups were performed. In  
990 these cases, a Bonferroni adjustment to alpha values was applied and the statistical  
991 significance was accepted at the  $p < 0.003$  level. In cases in which only the assumption  
992 of homoscedasticity was violated, a Welch's ANOVA followed by a Games-Howell  
993 post hoc was used to compare groups.

994

995

996

997

998

999

1000

1001

1002

1003 **Acknowledgments**

1004 The authors thank Lilian do Carmo Heck for the excellent technical assistance. This  
1005 work was funded by the São Paulo Research Foundation (FAPESP; grants  
1006 #2019/11196-0 and #2015/23467-7), CNPq, and PROPE-UNESP.

1007

1008 **Author contributions**

1009 P.L.K. and E.C. conceived and designed research. P.L.K. performed all in vivo  
1010 experiments. P.L.K. and I.P.L. performed immunofluorescence and in situ  
1011 hybridization. A.K. and J.P.M.L. performed ELISA. L.C.C.N. performed HPLC  
1012 measurements. P.L.K., I.P.L., A.K., and J.P.M.L. analyzed data. P.L.K., I.P.L., A.K.,  
1013 D.B.Z, and E.C. interpreted data. P.L.K. and A.K. drafted the manuscript. P.L.K., I.P.L.,  
1014 A.K., J.P.M.L., F.Q.C., L.C.C.N., J.V.M., D.B.Z., D.S.A.C., and E.C. edited and revised  
1015 the manuscript. P.L.K., I.P.L., A.K., J.P.M.L., F.Q.C., L.C.C.N, J.V.M., D.B.Z.,  
1016 D.S.A.C., and E.C. read and approved the final version of the manuscript.

1017

1018 **Competing interests**

1019 The authors declare no competing interests.

1020

1021 **Materials & correspondence**

1022 Correspondence and requests for materials should be addressed to P.L.K. and/or E.C.

1023

1024

1025

1026

1027

1028

1029

1030

1031

1032

1033

1034



1035 **REFERENCES**

1036

1037 Abe C, Inoue T, Inglis MA, Viar KE, Huang L, Ye H, Rosin DiL, Stornetta  
1038 RL, Okusa MD, Guyenet PG. 2017. C1 neurons mediate a stress-  
1039 induced anti-inflammatory reflex in mice. *Nature Neuroscience*  
1040 **20**:700–707. doi:10.1038/nn.4526

1041 Aicher SA, Saravay RH, Cravo S, Jeske I, Morrison SF, Reis DJ, Milner  
1042 TA. 1996. Monosynaptic projections from the nucleus tractus solitarii  
1043 to C1 adrenergic neurons in the rostral ventrolateral medulla:  
1044 Comparison with input from the caudal ventrolateral medulla. *Journal*  
1045 *of Comparative Neurology* **373**:62–75. doi:10.1002/(SICI)1096-  
1046 9861(19960909)373:1<62::AID-CNE6>3.0.CO;2-B

1047 Allen AM. 1998. Angiotensin AT1 receptor-mediated excitation of rat  
1048 carotid body chemoreceptor afferent activity. *Journal of Physiology*  
1049 **510**:773–781. doi:10.1111/j.1469-7793.1998.773bj.x

1050 Araujo LP, Maricato JT, Guerreschi MG, Takenaka MC, Nascimento VM,  
1051 de Melo FM, Quintana FJ, Brum PC, Basso AS. 2019. The  
1052 Sympathetic Nervous System Mitigates CNS Autoimmunity via  $\beta$ 2-  
1053 Adrenergic Receptor Signaling in Immune Cells. *Cell Reports*  
1054 **28**:3120-3130.e5. doi:10.1016/j.celrep.2019.08.042

1055 Asirvatham-Jeyaraj N, Gauthier MM, Banek CT, Ramesh A, Garver H,  
1056 Fink GD, Osborn JW. 2021. Renal Denervation and Celiac  
1057 Ganglionectomy Decrease Mean Arterial Pressure Similarly in  
1058 Genetically Hypertensive Schlager (BPH/2J) Mice. *Hypertension*  
1059 **519**–528. doi:10.1161/HYPERTENSIONAHA.119.14069

1060 Bassi GS, Dias DPM, Franchin M, Talbot J, Reis DG, Menezes GB,  
1061 Castania JA, Garcia-Cairasco N, Resstel LBM, Salgado HC, Cunha  
1062 FQ, Cunha TM, Ulloa L, Kanashiro A. 2017. Modulation of  
1063 experimental arthritis by vagal sensory and central brain stimulation.

- 1064 *Brain, Behavior, and Immunity* **64**:330–343.  
1065 doi:10.1016/j.bbi.2017.04.003
- 1066 Bassi GS, Kanashiro A, Coimbra NC, Terrando N, Maixner W, Ulloa L.  
1067 2020. Anatomical and clinical implications of vagal modulation of the  
1068 spleen. *Neuroscience and Biobehavioral Reviews* **112**:363–373.  
1069 doi:10.1016/j.neubiorev.2020.02.011
- 1070 Bautista LE, Vera LM, Arenas IA, Gamarra G. 2005. Independent  
1071 association between inflammatory markers ( C-reactive protein ,  
1072 interleukin-6 , and TNF- a ) and essential hypertension 149–154.  
1073 doi:10.1038/sj.jhh.1001785
- 1074 Borovikova L V., Ivanova S, Zhang M, Yang H, Botchkina GI, Watkins  
1075 LR, Wang H, Abumrad N, Eaton JW, Tracey KJ. 2000. Vagus nerve  
1076 stimulation attenuates the systemic inflammatory response to  
1077 endotoxin. *Nature* **405**:458–462. doi:10.1038/35013070
- 1078 Chang EH, Chavan SS, Pavlov VA. 2019. Cholinergic control of  
1079 inflammation, metabolic dysfunction, and cognitive impairment in  
1080 obesity-associated disorders: Mechanisms and novel therapeutic  
1081 opportunities. *Frontiers in Neuroscience* **13**:1–13.  
1082 doi:10.3389/fnins.2019.00263
- 1083 Chavan SS, Pavlov VA, Tracey KJ. 2017. Mechanisms and Therapeutic  
1084 Relevance of Neuro-immune Communication. *Immunity* **46**:927–942.  
1085 doi:10.1016/j.immuni.2017.06.008
- 1086 Chu C, Artis D, Chiu IM. 2020. Neuro-immune Interactions in the  
1087 Tissues. *Immunity* **52**:464–474. doi:10.1016/j.immuni.2020.02.017
- 1088 Colombari E, Menani J V, Talman WT. 1996. Commissural NTS  
1089 contributes to pressor responses to glutamate injected into the  
1090 medial NTS of awake rats. *American Journal of Physiology-  
1091 Regulatory, Integrative and Comparative Physiology* **270**:R1220–  
1092 R1225. doi:10.1152/ajpregu.1996.270.6.R1220

- 1093 Cruz J de C, Bonagamba LGH, Stern JE, Machado BH. 2010. Fos  
1094 expression in the NTS in response to peripheral chemoreflex  
1095 activation in awake rats. *Autonomic Neuroscience: Basic and Clinical*  
1096 **152**:27–34. doi:10.1016/j.autneu.2009.08.016
- 1097 da Silva EF, Bassi M, Menani JV, Colombari DSA, Zoccal DB, Pedrino  
1098 GR, Colombari E. 2019. Carotid bodies contribute to  
1099 sympathoexcitation induced by acute salt overload. *Experimental*  
1100 *Physiology* **104**:15–27. doi:<https://doi.org/10.1113/EP087110>
- 1101 Erickson JT, Millhorn DE. 1994. Hypoxia and electrical stimulation of the  
1102 carotid sinus nerve induce fos-like immunoreactivity within  
1103 catecholaminergic and serotonergic neurons of the rat brainstem.  
1104 *Journal of Comparative Neurology* **348**:161–182.  
1105 doi:10.1002/cne.903480202
- 1106 Fernández R, González S, Rey S, Cortés PP, Maisey KR, Reyes EP,  
1107 Larraín C, Zapata P. 2008. Lipopolysaccharide-induced carotid body  
1108 inflammation in cats: Functional manifestations, histopathology and  
1109 involvement of tumour necrosis factor- $\alpha$ . *Experimental Physiology*  
1110 **93**:892–907. doi:10.1113/expphysiol.2008.041152
- 1111 Ferreira CB, Cravo SL, Stocker SD. 2018. Airway obstruction produces  
1112 widespread sympathoexcitation: role of hypoxia, carotid  
1113 chemoreceptors, and NTS neurotransmission. *Physiological Reports*  
1114 **6**. doi:10.14814/phy2.13536
- 1115 Fonseca MT, Moretti EH, Marques LMM, MacHado BF, Brito CF,  
1116 Guedes JT, Komegae EN, Vieira TS, Festuccia WT, Lopes NP,  
1117 Steiner AA. 2021. A leukotriene-dependent spleen-liver axis drives  
1118 TNF production in systemic inflammation. *Science Signaling* **14**.  
1119 doi:10.1126/scisignal.abb0969
- 1120 Gabanyi I, Muller PA, Feighery L, Oliveira TY, Costa-pinto FA, Mucida D,  
1121 Gabanyi I, Muller PA, Feighery L, Oliveira TY, Costa-pinto FA,

- 1122 Mucida D. 2016. Neuro-immune Interactions Drive Tissue  
1123 Programming in Intestinal Macrophages Article Neuro-immune  
1124 Interactions Drive Tissue Programming in Intestinal Macrophages.  
1125 *Cell* **164**:378–391. doi:10.1016/j.cell.2015.12.023
- 1126 Garofalo MAR, Kettelhut IC, Roselino JES, Migliorini RH. 1996. Effect of  
1127 acute cold exposure on norpinephrine turnover rates in rat white  
1128 adipose tissue. *Journal of the Autonomic Nervous System* **60**:206–  
1129 208. doi:10.1016/0165-1838(96)00037-9
- 1130 Grieve AG, Xu H, Künzel U, Bambrough P, Sieber B, Freeman M. 2017.  
1131 Phosphorylation of iRhom2 at the plasma membrane controls  
1132 mammalian TACE-dependent inflammatory and growth factor  
1133 signalling. *eLife* **6**:1–22. doi:10.7554/eLife.23968
- 1134 Jendzjowsky NG, Roy A, Barioni NO, Kelly MM, Green FHY, Wyatt CN,  
1135 Pye RL, Tenorio-Lopes L, Wilson RJA. 2018. Preventing acute  
1136 asthmatic symptoms by targeting a neuronal mechanism involving  
1137 carotid body lysophosphatidic acid receptors. *Nature*  
1138 *Communications* **9**:1–15. doi:10.1038/s41467-018-06189-y
- 1139 Jendzjowsky NG, Roy A, Iftinca M, Barioni NO, Kelly MM, Herrington  
1140 BA, Visser F, Altier C, Wilson RJA. 2021. PKC $\epsilon$  stimulation of  
1141 TRPV1 orchestrates carotid body responses to asthmakines. *Journal*  
1142 *of Physiology* **599**:1335–1354. doi:10.1113/JP280749
- 1143 Kanashiro A, Sônego F, Ferreira RG, Castanheira FVS, Leite CA,  
1144 Borges VF, Nascimento DC, Cólón DF, Alves-Filho JC, Ulloa L,  
1145 Cunha FQ. 2017. Therapeutic potential and limitations of cholinergic  
1146 anti-inflammatory pathway in sepsis. *Pharmacological Research*  
1147 **117**:1–8. doi:10.1016/j.phrs.2016.12.014
- 1148 Katayama PL. 2016. Adrenaline and the carotid body during  
1149 hypoglycaemia: an amplifying mechanism? *Journal of Physiology*  
1150 **594**:7161–7162. doi:10.1113/JP273238

- 1151 Katayama PL, Castania JA, Dias DPM, Patel KP, Fazan R, Salgado HC.  
1152 2015. Role of Chemoreceptor Activation in Hemodynamic  
1153 Responses to Electrical Stimulation of the Carotid Sinus in  
1154 Conscious Rats. *Hypertension* **66**:598–603.  
1155 doi:10.1161/HYPERTENSIONAHA.115.05316
- 1156 Katayama PL, Castania JA, Fazan R, Salgado HC. 2019. Interaction  
1157 between baroreflex and chemoreflex in the cardiorespiratory  
1158 responses to stimulation of the carotid sinus/nerve in conscious rats.  
1159 *Autonomic Neuroscience: Basic and Clinical* **216**:17–24.  
1160 doi:10.1016/j.autneu.2018.12.001
- 1161 Kim SJ, Fong AY, Pilowsky PM, Abbott SBG. 2018. Sympathoexcitation  
1162 following intermittent hypoxia in rat is mediated by circulating  
1163 angiotensin II acting at the carotid body and subfornical organ.  
1164 *Journal of Physiology* **596**:3217–3232. doi:10.1113/JP275804
- 1165 Kline DD, King TL, Austgen JR, Heesch CM, Hasser EM. 2010. Sensory  
1166 afferent and hypoxia-mediated activation of nucleus tractus solitarius  
1167 neurons that project to the rostral ventrolateral medulla.  
1168 *Neuroscience* **167**:510–527.  
1169 doi:10.1016/j.neuroscience.2010.02.012
- 1170 Koshiya N, Guyenet PG. 1996. Tonic sympathetic chemoreflex after  
1171 blockade of respiratory rhythmogenesis in the rat. *Journal of*  
1172 *Physiology* **491**:859–869. doi:10.1113/jphysiol.1996.sp021263
- 1173 Kox M, Van Eijk LT, Zwaag J, Van Den Wildenberg J, Sweep FCGJ,  
1174 Van Der Hoeven JG, Pickkers P. 2014. Voluntary activation of the  
1175 sympathetic nervous system and attenuation of the innate immune  
1176 response in humans. *Proceedings of the National Academy of*  
1177 *Sciences of the United States of America* **111**:7379–7384.  
1178 doi:10.1073/pnas.1322174111
- 1179 Kressel AM, Tsaava T, Levine YA, Chang EH, Addorizio ME, Chang Q,



- 1180 Burbach BJ, Carnevale D, Lembo G, Zador AM, Andersson U,  
1181 Pavlov VA, Chavan SS, Tracey KJ. 2020. Identification of a  
1182 brainstem locus that inhibits tumor necrosis factor. *Proceedings of*  
1183 *the National Academy of Sciences of the United States of America*  
1184 **117**:29803–29810. doi:10.1073/pnas.2008213117
- 1185 Kumar P, Prabhakar NR. 2012. Peripheral chemoreceptors: Function  
1186 and plasticity of the carotid body. *Comprehensive Physiology* **2**:141–  
1187 219. doi:10.1002/cphy.c100069
- 1188 Lankadeva YR, May CN, McKinley MJ, Neeland MR, Ma S, Hocking DM,  
1189 Robins-Browne R, Bedoui S, Farmer DGS, Bailey SR, Martelli D,  
1190 McAllen RM. 2020. Sympathetic nerves control bacterial clearance.  
1191 *Scientific Reports* **10**:1–8. doi:10.1038/s41598-020-72008-4
- 1192 Li DJ, Evans RG, Yang ZW, Song SW, Wang P, Ma XJ, Liu C, Xi T, Su  
1193 DF, Shen FM. 2011. Dysfunction of the cholinergic anti-inflammatory  
1194 pathway mediates organ damage in hypertension. *Hypertension*  
1195 **57**:298–307. doi:10.1161/HYPERTENSIONAHA.110.160077
- 1196 Li M, Galligan J, Wang D, Fink G. 2010. The effects of celiac  
1197 ganglionectomy on sympathetic innervation to the splanchnic organs  
1198 in the rat. *Autonomic Neuroscience: Basic and Clinical* **154**:66–73.  
1199 doi:10.1016/j.autneu.2009.11.009
- 1200 Luise King T, Heesch CM, Clark CG, Kline DD, Hasser EM. 2012.  
1201 Hypoxia activates nucleus tractus solitarii neurons projecting to the  
1202 paraventricular nucleus of the hypothalamus. *American Journal of*  
1203 *Physiology - Regulatory Integrative and Comparative Physiology*  
1204 **302**. doi:10.1152/ajpregu.00028.2012
- 1205 Ma Y, Zhao S, Shen S, Fang S, Ye Z, Shi Z, Hong A. 2015. A novel  
1206 recombinant slow-release TNF  $\alpha$ -derived peptide effectively inhibits  
1207 tumor growth and angiogenesis. *Scientific Reports* **5**:1–17.  
1208 doi:10.1038/srep13595

- 1209 Malheiros-Lima MR, Silva JN, Souza FC, Takakura AC, Moreira TS.  
1210 2020. C1 neurons are part of the circuitry that recruits active  
1211 expiration in response to peripheral chemoreceptors activation. *eLife*  
1212 **9**:1–23. doi:10.7554/eLife.52572
- 1213 Marcus NJ, Del Rio R, Schultz EP, Xia X-H, Schultz HD. 2014. Carotid  
1214 body denervation improves autonomic and cardiac function and  
1215 attenuates disordered breathing in congestive heart failure. *The*  
1216 *Journal of Physiology* **592**:391–408.  
1217 doi:10.1113/jphysiol.2013.266221
- 1218 Martelli D, Yao ST, Mckinley MJ, Mcallen RM. 2014. Reflex control of  
1219 inflammation by sympathetic nerves, not the vagus. *Journal of*  
1220 *Physiology* **592**:1677–1686. doi:10.1113/jphysiol.2013.268573
- 1221 McBryde FD, Abdala AP, Hendy EB, Pijacka W, Marvar P, Moraes DJA,  
1222 Sobotka PA, Paton JFR. 2013. The carotid body as a putative  
1223 therapeutic target for the treatment of neurogenic hypertension.  
1224 *Nature Communications* **4**:1–11. doi:10.1038/ncomms3395
- 1225 Melo MR, Gasparini S, Speretta GF, Silva EF, Rodrigues Pedrino G,  
1226 Menani J V, Zoccal DB, Colombari DSA, Colombari E. 2019.  
1227 Importance of the commissural nucleus of the solitary tract in  
1228 renovascular hypertension. *Hypertension Research* **42**:587–597.  
1229 doi:10.1038/s41440-018-0190-6
- 1230 Mkrtchian S, Kåhlin J, Ebberyd A, Gonzalez C, Sanchez D, Balbir A,  
1231 Kostuk EW, Shirahata M, Fagerlund MJ, Eriksson LI. 2012. The  
1232 human carotid body transcriptome with focus on oxygen sensing and  
1233 inflammation - a comparative analysis. *Journal of Physiology*  
1234 **590**:3807–3819. doi:10.1113/jphysiol.2012.231084
- 1235 Morrison SF. 2001. Differential control of sympathetic outflow. *American*  
1236 *Journal of Physiology - Regulatory Integrative and Comparative*  
1237 *Physiology* **281**. doi:10.1152/ajpregu.2001.281.3.r683

- 1238 Murray K, Rude KM, Sladek J, Reardon C. 2021. Divergence of  
1239 neuroimmune circuits activated by afferent and efferent vagal nerve  
1240 stimulation in the regulation of inflammation. *Journal of Physiology*  
1241 **599**:2075–2084. doi:10.1113/JP281189
- 1242 Nardocci G, Martin A, Abarzúa S, Rodríguez J, Simon F, Reyes EP,  
1243 Acuña-Castillo C, Navarro C, Cortes PP, Fernández R. 2015. Sepsis  
1244 progression to multiple organ dysfunction in carotid chemo/baro-  
1245 denervated rats treated with lipopolysaccharide. *Journal of*  
1246 *Neuroimmunology* **278**:44–52. doi:10.1016/j.jneuroim.2014.12.002
- 1247 Narkiewicz K, Ratcliffe LEK, Hart EC, Briant LJB, Chrostowska M, Wolf  
1248 J, Szyndler A, Hering D, Abdala AP, Manghat N, Burchell AE, Durant  
1249 C, Lobo MD, Sobotka PA, Patel NK, Leiter JC, Engelman ZJ,  
1250 Nightingale AK, Paton JFR. 2016. Unilateral Carotid Body Resection  
1251 in Resistant Hypertension: A Safety and Feasibility Trial. *JACC:*  
1252 *Basic to Translational Science* **1**:313–324.  
1253 doi:10.1016/j.jacbts.2016.06.004
- 1254 Neff RA, Mihalevich M, Mendelowitz D. 1998. Stimulation of NTS  
1255 activates NMDA and non-NMDA receptors in rat cardiac vagal  
1256 neurons in the nucleus ambiguus. *Brain Research* **792**:277–282.  
1257 doi:10.1016/S0006-8993(98)00149-8
- 1258 Niewinski P, Janczak D, Rucinski A, Tubek S, Engelman ZJ, Piesiak P,  
1259 Jazwiec P, Banasiak W, Fudim M, Sobotka PA, Javaheri S, Hart  
1260 ECJ, Paton JFR, Ponikowski P. 2017. Carotid body resection for  
1261 sympathetic modulation in systolic heart failure: results from first-in-  
1262 man study. *European Journal of Heart Failure* **19**:391–400.  
1263 doi:10.1002/ejhf.641
- 1264 Norlander AE, Madhur MS, Harrison DG. 2018. The immunology of  
1265 hypertension *The Journal of Experimental Medicine* 21–34.
- 1266 Paxinos G, Charles Watson. 2007. *The Rat Brain in Stereotaxic*

- 1267           Coordinates Sixth Edition, Elsevier Academic Press.
- 1268 Pijacka W, Katayama PL, Salgado HC, Lincevicius GS, Campos RR,  
1269           Mcbryde FD, Paton JFR, Schultz H, Powell F. 2018. Variable role of  
1270           carotid bodies in cardiovascular responses to exercise , hypoxia and  
1271           hypercapnia in spontaneously hypertensive rats **00**:1–16.  
1272           doi:10.1113/JP275487
- 1273 Rauchhaus M, Doehner W, Francis DP, Davos C, Kemp M, Liebenthal  
1274           C, Niebauer J, Hooper J, Volk HD, Coats AJS, Anker SD. 2000.  
1275           Plasma cytokine parameters and mortality in patients with chronic  
1276           heart failure. *Circulation* **102**:3060–3067.  
1277           doi:10.1161/01.CIR.102.25.3060
- 1278 Schultz HD, Li YL, Ding Y. 2007. Arterial chemoreceptors and  
1279           sympathetic nerve activity: Implications for hypertension and heart  
1280           failure. *Hypertension* **50**:6–13.  
1281           doi:10.1161/HYPERTENSIONAHA.106.076083
- 1282 Sesso HD, Jiménez MC, Wang L, Ridker PM, Buring JE, Michael  
1283           Gaziano J. 2015. Plasma inflammatory markers and the risk of  
1284           developing hypertension in men. *Journal of the American Heart*  
1285           *Association* **4**:1–9. doi:10.1161/JAHA.115.001802
- 1286 Shin MK, Eraso CC, Mu YP, Gu C, Yeung BHY, Kim LJ, Liu XR, Wu ZJ,  
1287           Paudel O, Pichard LE, Shirahata M, Tang WY, Sham JSK, Polotsky  
1288           VY. 2019. Leptin Induces Hypertension Acting on Transient  
1289           Receptor Potential Melastatin 7 Channel in the Carotid Body.  
1290           *Circulation Research* **125**:989–1002.  
1291           doi:10.1161/CIRCRESAHA.119.315338
- 1292 Shu HF, Wang BR, Wang SR, Yao W, Huang HP, Zhou Z, Wang X, Fan  
1293           J, Wang T, Ju G. 2007. IL-1 $\beta$  inhibits IK and increases [Ca<sup>2+</sup>]<sub>i</sub> in the  
1294           carotid body glomus cells and increases carotid sinus nerve firings in  
1295           the rat. *European Journal of Neuroscience* **25**:3638–3647.

- 1296 doi:10.1111/j.1460-9568.2007.05586.x
- 1297 Simó R, Barbosa-Desongles A, Lecube A, Hernandez C, Selva DM.  
1298 2012. Potential role of tumor necrosis factor- $\alpha$  in downregulating sex  
1299 hormone-binding globulin. *Diabetes* **61**:372–382. doi:10.2337/db11-  
1300 0727
- 1301 Steinman L. 2004. Elaborate interactions between the immune and  
1302 nervous systems. *Nature Immunology* **5**:575–581.  
1303 doi:10.1038/ni1078
- 1304 Tanaka S, Abe C, Abbott SBG, Zheng S, Yamaoka Y, Lipsey JE,  
1305 Skrypnik NI, Yao J, Inoue T, Nash WT, Stornetta DS, Rosin DL,  
1306 Stornetta RL, Guyenet PG, Okusa MD. 2021. Vagus nerve  
1307 stimulation activates two distinct neuroimmune circuits converging in  
1308 the spleen to protect mice from kidney injury. *Proceedings of the  
1309 National Academy of Sciences of the United States of America*  
1310 **118**:1–12. doi:10.1073/PNAS.2021758118
- 1311 Thompson EL, Ray CJ, Holmes AP, Pye RL, Wyatt CN, Coney AM,  
1312 Kumar P. 2016. Adrenaline release evokes hyperpnoea and an  
1313 increase in ventilatory CO<sub>2</sub> sensitivity during hypoglycaemia: a role  
1314 for the carotid body. *Journal of Physiology* **594**:4439–4452.  
1315 doi:10.1113/JP272191
- 1316 Tromp TR, Mahesh D, Joles JA, Ramchandra R. 2018. Direct recording  
1317 of cardiac and renal sympathetic nerve activity shows differential  
1318 control in renovascular hypertension. *Hypertension* **71**:1108–1116.  
1319 doi:10.1161/HYPERTENSIONAHA.117.10749
- 1320 van Maanen MA, Vervoordeldonk MJ, Tak PP. 2009. The cholinergic  
1321 anti-inflammatory pathway: Towards innovative treatment of  
1322 rheumatoid arthritis. *Nature Reviews Rheumatology* **5**:229–232.  
1323 doi:10.1038/nrrheum.2009.31
- 1324 van Westerloo DJ, Choi G, Löwenberg EC, Truijien J, de Vos AF, Endert



- 1325 E, Meijers JCM, Zhou L, Pereira MPFL, Queiroz KCS, Diks SH, Levi  
1326 M, Peppelenbosch MP, van der Poll T. 2011. Acute stress elicited by  
1327 bungee jumping suppresses human innate immunity. *Molecular*  
1328 *Medicine* **17**:180–188. doi:10.2119/molmed.2010.00204
- 1329 Wang X, Wang BR, Duan XL, Zhang P, Ding YQ, Jia Y, Jiao XY, Ju G.  
1330 2002. Strong expression of interleukin-1 receptor type I in the rat  
1331 carotid body. *Journal of Histochemistry and Cytochemistry* **50**:1677–  
1332 1684. doi:10.1177/002215540205001213
- 1333 Watkins LR, Goehler LE, Relton JK, Tartaglia N, Silbert L, Martin D,  
1334 Maier SF. 1995. Blockade of interleukin-1 induced hyperthermia by  
1335 subdiaphragmatic vagotomy: evidence for vagal mediation of  
1336 immune-brain communication. *Neuroscience Letters* **183**:27–31.  
1337 doi:10.1016/0304-3940(94)11105-R
- 1338 Wei S, Zhang Z, Beltz TG, Yu Y, Johnson AK, Felder RB. 2013.  
1339 Subfornical Organ Mediates Sympathetic and Hemodynamic  
1340 Responses to Blood-Borne Proinflammatory Cytokines 118–125.  
1341 doi:10.1161/HYPERTENSIONAHA.113.01404
- 1342 Willis A, Mihalevich M, Neff RA, Mendelowitz D. 1996. Three types of  
1343 postsynaptic glutamatergic receptors are activated in DMNX neurons  
1344 upon stimulation of NTS. *American Journal of Physiology -*  
1345 *Regulatory Integrative and Comparative Physiology* **271**.  
1346 doi:10.1152/ajpregu.1996.271.6.r1614
- 1347 Yuan G, Peng YJ, Khan SA, Nanduri J, Singh A, Vasavda C, Semenza  
1348 GL, Kumar GK, Snyder SH, Prabhakar NR. 2016. H<sub>2</sub>S production by  
1349 reactive oxygen species in the carotid body triggers hypertension in  
1350 a rodent model of sleep apnea. *Science Signaling* **9**:1–11.  
1351 doi:10.1126/scisignal.aaf3204
- 1352 Zera T, Moraes DJA, da Silva MP, Fisher JP, Paton JFR. 2019. The  
1353 Logic of Carotid Body Connectivity to the Brain. *Physiology* **34**:264–

1354           282. doi:10.1152/physiol.00057.2018  
1355   Zhang ZH, Wei SG, Francis J, Felder RB. 2003. Cardiovascular and  
1356           renal sympathetic activation by blood-borne TNF- $\alpha$  in rat: The role of  
1357           central prostaglandins. *American Journal of Physiology - Regulatory*  
1358           *Integrative and Comparative Physiology* **284**:916–927.  
1359           doi:10.1152/ajpregu.00406.2002

1360

1361

1362

1363

1364

1365

1366

1367

1368

1369

1370

1371

1372

1373

1374

1375

1376

1377

1378

1379

1380

1381

1382

1383

1384

1385

1386

1387

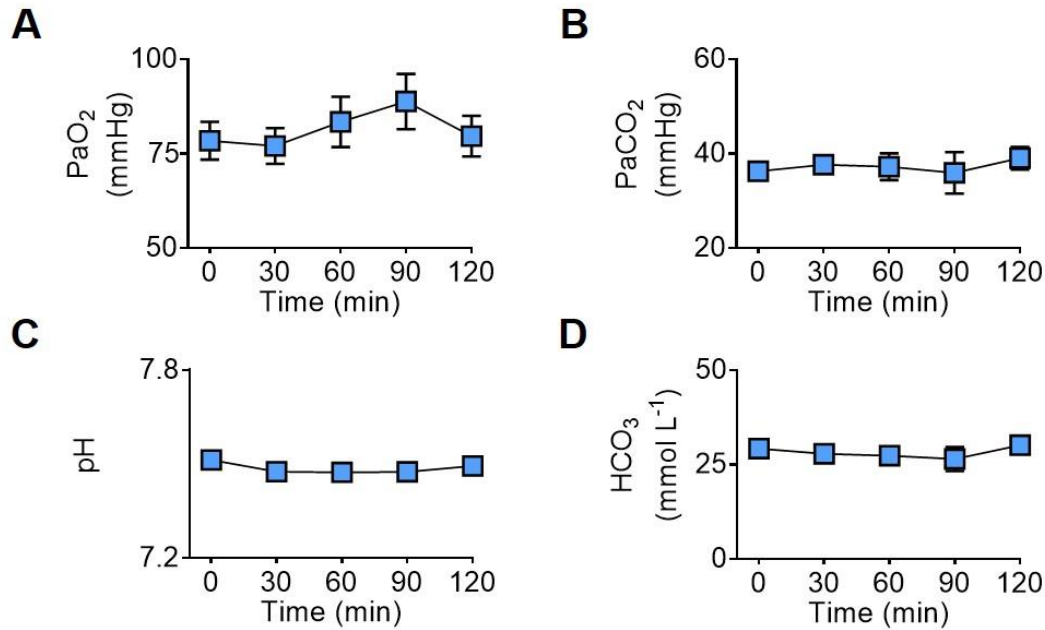
1388  
1389  
1390  
1391  
1392  
1393  
  
1394  
  
1395  
1396  
1397  
1398  
1399  
1400  
1401  
1402  
1403  
1404  
  
1405  
1406  
1407  
1408  
1409  
1410  
1411  
1412  
1413  
1414  
1415  
1416  
1417  
1418  
1419  
1420  
1421  
1422  
1423  
1424  
1425  
1426  
1427  
1428  
1429

## Supplementary Information

### The Carotid Body Detects Circulating Tumor Necrosis Factor-Alpha to Activate a Sympathetic Anti-Inflammatory Reflex

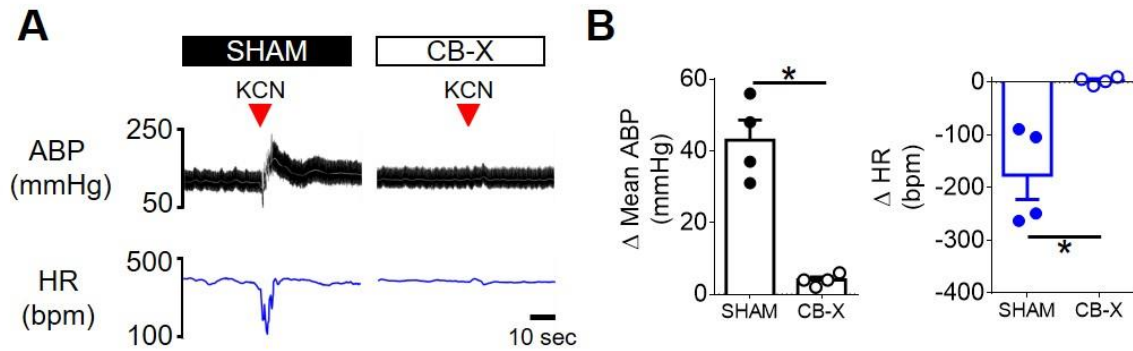
Pedro L. Katayama<sup>1</sup>, Isabela P. Leirão<sup>1</sup>, Alexandre Kanashiro<sup>2</sup>, João Paulo M. Luiz<sup>2</sup>, Fernando Q. Cunha<sup>2</sup>, Luiz C. C. Navegantes<sup>3</sup>, Jose V. Menani<sup>1</sup>, Daniel B. Zoccal<sup>1</sup>, Débora S. A. Colombari<sup>1</sup> & Eduardo Colombari<sup>1</sup>

**Affiliations:** <sup>1</sup>Department of Physiology and Pathology, School of Dentistry, São Paulo State University, Araraquara, São Paulo, Brazil. <sup>2</sup>Department of Pharmacology, Ribeirão Preto Medical School, University of São Paulo, Ribeirão Preto, São Paulo, Brazil. <sup>3</sup>Department of Physiology, Ribeirão Preto Medical School, University of São Paulo, Ribeirão Preto, São Paulo, Brazil.



1430  
1431  
1432  
1433  
1434  
1435  
1436  
1437  
1438  
1439  
1440  
1441  
1442  
1443  
1444  
1445  
1446  
1447  
1448  
1449  
1450  
1451  
1452  
1453  
1454  
1455  
1456

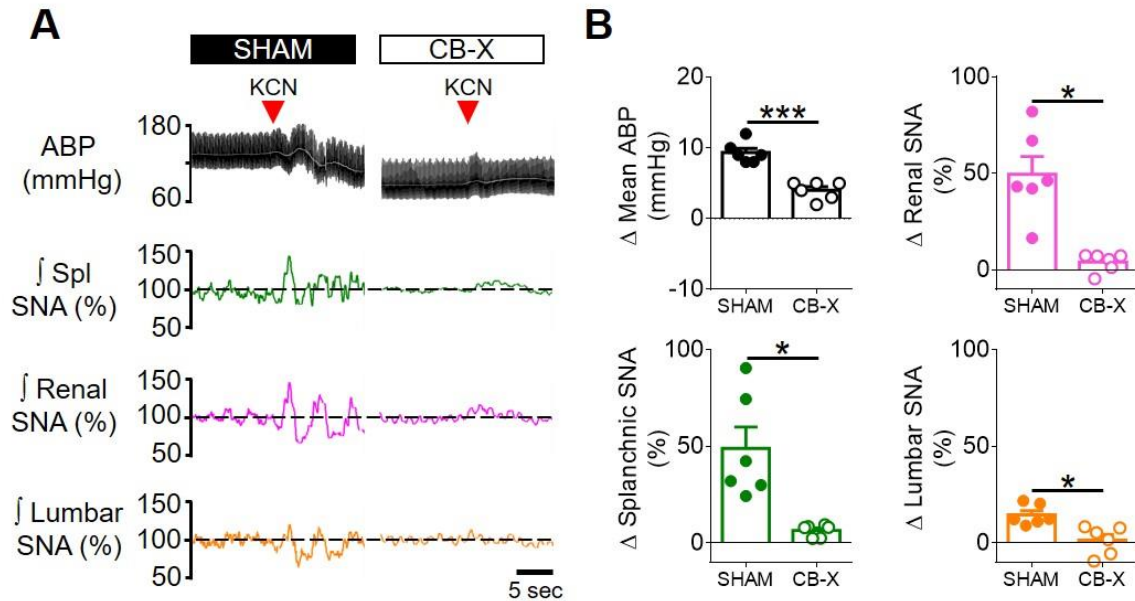
**Figure supplement 1.** Acute intravenous TNF- $\alpha$  does not affect arterial blood gases, pH, and bicarbonate. All measures were performed using a I-STAT device with CG4+ cartridges (Abbott, Abbott Park, IL, USA). **A – D.** Summary data ( $n = 5$ ) showing that the intravenous administration of TNF- $\alpha$  (500 ng) did not affect the partial pressure of oxygen (PaO<sub>2</sub>), the partial pressure of carbon dioxide (PaCO<sub>2</sub>), the pH, and the bicarbonate (HCO<sub>3</sub><sup>-</sup>) concentration in the arterial blood of unanesthetized, spontaneously breathing rats. One-way repeated measures ANOVA: PaO<sub>2</sub>,  $F_{(1.525, 6.102)} = 1.659$ ,  $p = 0.259$ ,  $\epsilon = 0.381$ ; PaCO<sub>2</sub>,  $F_{(4,16)} = 0.370$ ,  $p = 0.826$ ; pH,  $F_{(4,16)} = 2.838$ ,  $p = 0.059$ ; HCO<sub>3</sub><sup>-</sup>,  $F_{(1.879, 7.515)} = 1.207$ ,  $p = 0.347$ ,  $\epsilon = 0.470$ . Data are means  $\pm$  SEM.



1457  
1458  
1459  
1460  
1461  
1462  
1463  
1464  
1465  
1466  
1467  
1468  
1469  
1470  
1471  
1472  
1473  
1474  
1475  
1476  
1477  
1478  
1479  
1480  
1481  
1482  
1483  
1484  
1485  
1486  
1487  
1488

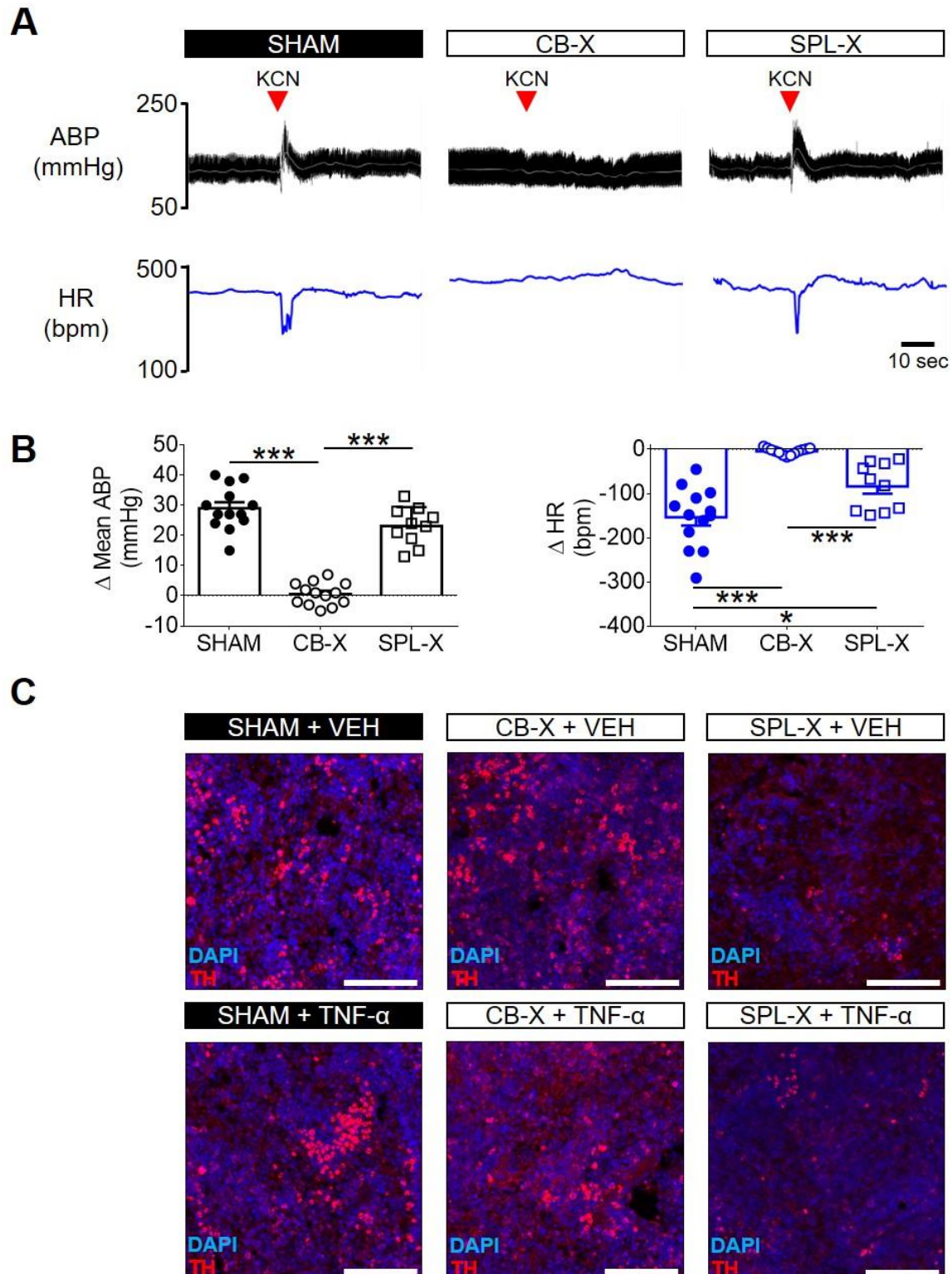
**Figure supplement 2.** Verification of carotid body ablation in *experiment 3*. **A.** Representative tracings of arterial blood pressure (pulsatile ABP, black; mean ABP, white) and heart rate (HR; blue) of a SHAM rat (left) and of a CB-X rat (right) in response to KCN (red arrowhead, 40  $\mu$ g, IV) under unanesthetized conditions. **B.** Summary data showing the peak changes in mean ABP and HR in response to KCN from SHAM (filled symbols, n = 4) and CB-X (open symbols, n = 4) rats. The cardiovascular responses to carotid body stimulation by intravenous KCN were abolished in CB-X rats, confirming the efficacy of bilateral carotid body ablation:  $\Delta$  mean ABP (SHAM,  $43 \pm 6$  mmHg; CB-X,  $4 \pm 1$  mmHg;  $t(3.128) = 6.912$ ,  $p = 0.005$ , Welch's *t*-test),  $\Delta$  HR (SHAM,  $-176 \pm 46$  bpm; CB-X,  $3 \pm 3$  bpm;  $t(3.033) = -3.866$ ,  $p = 0.03$ , Welch's *t*-test). \* $p < 0.05$ . Data are means  $\pm$  SEM.





1489  
 1490 **Figure supplement 3.** Verification of carotid body ablation at the end of *experiment 4*. **A.**  
 1491 Representative tracings of arterial blood pressure (pulsatile ABP, black; mean ABP, white), splanchnic  
 1492 SNA (Spl; green), renal SNA (magenta) and lumbar SNA (orange) of a SHAM rat (left) and of a CB-X  
 1493 rat (right) in response to KCN (red arrowhead, 40  $\mu$ g, IV) under anesthetized conditions. **B.** Summary  
 1494 data showing the changes in mean ABP, Splanchnic SNA, Renal SNA and Lumbar SNA in response  
 1495 to KCN from SHAM (filled symbols, n = 6) and CB-X (open symbols, n = 6) rats. For each rat, baseline  
 1496 rectified and integrated SNA was normalized to 100% and the peak changes in response to KCN were  
 1497 calculated. The sympathetic and blood pressure responses to KCN were significantly attenuated in CB-  
 1498 X rats, confirming the efficacy of bilateral carotid body ablation:  $\Delta$  Spl SNA (SHAM,  $48 \pm 11$  %; CB-X,  $7$   
 1499  $\pm 1$  %;  $U = 0$ ,  $z = -2.882$ ,  $p = 0.002$ , Mann-Whitney  $U$ -test),  $\Delta$  Renal SNA (SHAM,  $50 \pm 9$  %; CB-X,  $4 \pm$   
 1500  $2$  %;  $t(5.452) = 4.815$ ,  $p = 0.004$ , Welch's  $t$ -test),  $\Delta$  Lumbar SNA (SHAM,  $15 \pm 2$  %; CB-X,  $1 \pm 3$  % ;  
 1501  $t(10) = 3.547$ ,  $p = 0.005$ , Student's  $t$ -test), and  $\Delta$  Mean ABP (SHAM,  $9 \pm 1$  mmHg; CB-X,  $4 \pm 1$  % ;  $t(10)$   
 1502  $= 6.644$ ,  $p < 0.001$ , Student's  $t$ -test). \* $p < 0.05$  and \*\*\* $p < 0.001$ . Data are means  $\pm$  SEM.

1503  
 1504  
 1505  
 1506  
 1507  
 1508  
 1509  
 1510  
 1511  
 1512  
 1513  
 1514  
 1515  
 1516  
 1517



1518  
1519  
1520  
1521  
1522  
1523  
1524  
1525  
1526  
1527

**Figure supplement 4.** Verification of carotid body ablation and splanchnic sympathetic denervation in *experiment 5*. **A.** Representative tracings of arterial blood pressure (pulsatile ABP, black; mean ABP, white) and heart rate (HR; blue) of a SHAM rat (left), of a CB-X rat (middle), and of a SPL-X rat (right) in response to KCN (red arrowhead, 40  $\mu$ g, IV) under unanesthetized conditions. **B.** Summary data showing the peak changes in mean ABP (black graphs, left) and HR (blue graphs, right) in response to KCN from SHAM (filled circles,  $n = 13$ ), CB-X (open circles,  $n = 13$ ), and SPL-X (open squares,  $n = 10$ ) rats. The cardiovascular (mean ABP and HR) responses to carotid body stimulation by intravenous KCN were abolished in CB-X rats, confirming the efficacy of bilateral carotid body ablation:  $\Delta$  mean ABP (SHAM,  $29 \pm 2$  mmHg; CB-X,  $1 \pm 1$  mmHg; SPL-X,  $23 \pm 2$ ) and  $\Delta$  mean HR (SHAM,  $-154 \pm 19$  bpm;

1528 CB-X,  $-4 \pm 2$  bpm; SPL-X,  $-84 \pm 17$ ). Regarding  $\Delta$  mean ABP, a one-way ANOVA detected statistically  
1529 significant differences between groups,  $F_{(2, 33)} = 83.134$ ,  $p < 0.001$ . Subsequent post hoc analysis with  
1530 a Bonferroni adjustment revealed that the mean difference in  $\Delta$  mean ABP between CB-X and SHAM  
1531 rats was statistically significant ( $-28$  mmHg, 95% CI  $[-34, -23]$ ,  $p < 0.001$ ) as well as the mean difference  
1532 in  $\Delta$  mean ABP between CB-X and SPL-X rats ( $-22$  mmHg, 95% CI  $[-29, -16]$ ,  $p < 0.001$ ). Regarding  $\Delta$   
1533 HR, a Welch ANOVA detected statistically significant differences between groups,  $F_{(2, 14.078)} = 40.040$ ,  
1534  $p < 0.001$ . Games-Howell post hoc analysis revealed that the mean difference in  $\Delta$  HR between CB-X  
1535 and SHAM rats was statistically significant (149 bpm, 95% CI  $[99, 200]$ ,  $p < 0.001$ ) as well as the mean  
1536 difference in  $\Delta$  mean HR between CB-X and SPL-X rats (79 bpm, 95% CI  $[33, 126]$ ,  $p = 0.003$ ). In  
1537 addition, the mean difference in  $\Delta$  mean HR between SHAM and SPL-X rats was also statistically  
1538 significant ( $-70$  bpm, 95% CI  $[-133, -7]$ ,  $p = 0.029$ ). \* $p < 0.05$  and \*\*\* $p < 0.001$ . Data are means  $\pm$  SEM.  
1539 **C.** Representative images of spleen sections from one animal of each group obtained at the end of  
1540 *experiment 5* and processed for nuclear staining (DAPI, blue) and tyrosine hydroxylase (TH, red). Note  
1541 that TH staining is substantially less pronounced in the animals subjected to splanchnic sympathetic  
1542 denervation (SPL-X + VEH, upper right panel; and SPL-X + TNF- $\alpha$ , bottom right panel) as compared to  
1543 SHAM (SHAM + VEH, upper left panel; and SHAM + TNF- $\alpha$ , bottom left panel) and CB-X (CB-X +VEH,  
1544 upper middle panel; and CB-X + TNF- $\alpha$ , bottom middle panel). VEH, vehicle. Scale bars: 100  $\mu$ m.